

Review

A Comparative Review on the Catalytic Mechanism of Nonheme Iron Hydroxylases and Halogenases

Amy Timmins and Sam P. de Visser * 

Manchester Institute of Biotechnology and School of Chemical Engineering and Analytical Science,
The University of Manchester, 131 Princess Street, Manchester M1 7DN, UK;
amy.timmins@postgrad.manchester.ac.uk

* Correspondence: sam.devisser@manchester.ac.uk; Tel.: +44-161-306-4882

Received: 17 July 2018; Accepted: 30 July 2018; Published: 31 July 2018



Abstract: Enzymatic halogenation and haloperoxidation are unusual processes in biology; however, a range of halogenases and haloperoxidases exist that are able to transfer an aliphatic or aromatic C–H bond into C–Cl/C–Br. Haloperoxidases utilize hydrogen peroxide, and in a reaction with halides (Cl^-/Br^-), they react to form hypohalides ($\text{OCl}^-/\text{OBr}^-$) that subsequently react with substrate by halide transfer. There are three types of haloperoxidases, namely the iron-heme, nonheme vanadium, and flavin-dependent haloperoxidases that are reviewed here. In addition, there are the nonheme iron halogenases that show structural and functional similarity to the nonheme iron hydroxylases and form an iron(IV)-oxo active species from a reaction of molecular oxygen with α -ketoglutarate on an iron(II) center. They subsequently transfer a halide (Cl^-/Br^-) to an aliphatic C–H bond. We review the mechanism and function of nonheme iron halogenases and hydroxylases and show recent computational modelling studies of our group on the hectochlorin biosynthesis enzyme and prolyl-4-hydroxylase as examples of nonheme iron halogenases and hydroxylases. These studies have established the catalytic mechanism of these enzymes and show the importance of substrate and oxidant positioning on the stereo-, chemo- and regioselectivity of the reaction that takes place.

Keywords: inorganic reaction mechanisms; density functional theory; computational modelling; enzyme catalysis; quantum mechanics/molecular mechanics

1. Introduction

Nature utilizes enzymes for essential biochemical transformations, whereby compounds that cannot be taken in from food are synthesized. In addition, enzymatic processes often involve the biodegradation of toxic compounds, and as such, they contribute to vital biochemical mechanisms in the body. Structurally, enzymes are built up from proteins and contain an active site, where substrate and oxidant are brought together to initiate a chemical reaction. Although not specifically common in nature, there are a number of enzymes linked to halogenation and haloperoxidase reaction mechanisms, whereby an aliphatic or aromatic C–H bond is replaced by C–X ($X = \text{Cl}, \text{Br}, \text{I}$). This review will cover recent advances in the understanding of halogenases and haloperoxidases and specifically highlight how computational modelling can assist in elucidating the catalytic reaction mechanism of these enzymes. In the first few sections, we will cover the structure and catalytic cycles of typical halogenases and haloperoxidases in nature, while in the second part of this review, recent studies from our group on nonheme iron halogenases and hydroxylases are discussed.

Incorporating halogen atoms (fluoride, chloride, bromide, and iodide) into various natural product scaffolds is made possible through enzymes called halogenases, which are found in several marine and terrestrial organisms. Halogenases found in marine organisms typically use bromide as their halogen source, whereas those found in terrestrial organisms utilize chloride more commonly. This is despite

there being larger concentrations of chloride than bromide in seawater [1–3]. The biosynthesized halogenated compounds (organohalogens) in these organisms have a range of biochemical functions, including growth, reproduction and defense [1,3–6]. Furthermore, organohalogens have been shown to have many biological and medical properties, such as antibacterial, antifungal, antiviral, anti-inflammatory, anti-proliferative, anti-fouling, anti-feedant, cytotoxic, ichthyotoxic, and insecticidal activity [7] and as a result, many of today's best-selling herbicides, pesticides, and insecticides contain halogen atoms [8,9]. Importantly, often the biological and medical properties are lost when the halide substituent is removed. Thus, vancomycin loses its antibiotic activity when the aryl chloride functional groups are substituted for styryl groups [10].

The biological and medical properties of halogenated natural products, as previously stated, are often associated with the properties of the C–H bond itself. In the past, the role of the halogen in organohalogens was thought to only modulate the lipophilicity. In addition, in organohalogen compounds the halogen atom can form weak hydrogen bonding interactions with protein residues or alternatively function as a nucleophile. These halogen bonds may have importance for protein stability and folding as they have been shown to form through intermolecular interactions with proteins, similar to hydrogen bonds [11,12]. Consequently, it is a well-established practice within medicinal chemistry to introduce halogens into compounds because they are electron-withdrawing groups that do not significantly disrupt the size and shape of the molecule, and hence can bind as inhibitors easily. One halogen atom of great significance to the pharmaceutical industry is fluorine, because of its small size and its large electronegativity value. In fact, the combination of those two factors, plus their influence on lipophilicity, has resulted in some of the bestselling pharmaceuticals containing fluorine, as shown in Figure 1.

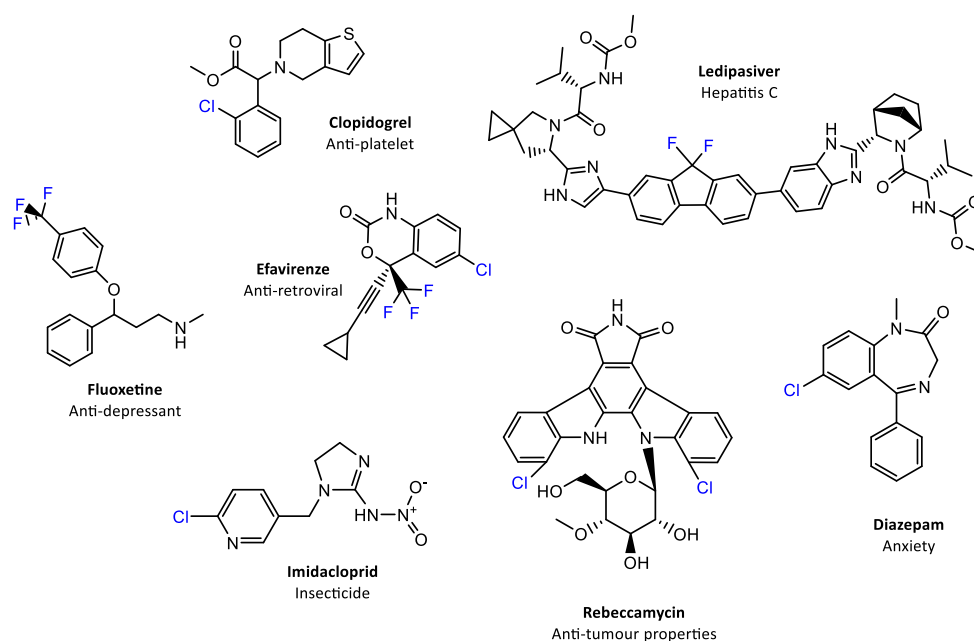


Figure 1. Examples of top-selling halogen-containing pharmaceuticals, agrochemicals, and halogenated natural products with known biological activities.

Additionally, the materials industry is interested in halogen-containing compounds as polymers, as they appear particularly well-suited for the design of smart devices, the development of nanotechnologies, organic semi-conductors, and lithium-ion batteries [13–15]. These developments are paving the way for next-generation materials. Given the increasing importance to selectively install halogens onto compounds for the pharmaceutical, agrochemical, and materials industries, several methods, rooted in organic chemistry, have been created. Traditionally, however, these methods require

materials which are toxic to the environment and result in poor selectivity, and despite steps taken to address these issues, for example, using directing groups to control the selectivity by controlling the position of functionalization, there is still a need to develop more sustainable ways of selectively halogenating compounds. One attractive method of doing this is to use halogenases, which are enzymes which selectively halogenate compounds during the production of secondary metabolites, to install halogens onto natural and synthetic scaffolds. Therefore, understanding the specific factors relating to their regio-, stereo-, and chemoselectivity of halogenases will open them up to applications in biotechnology and drug development, providing a greener and more selective process to the creation of organohalogenes.

1.1. Classification of Halogenases

There are five different types of halogenases/haloperoxidases known in the literature that all have been discovered over the past 50 years. They are grouped according to the nature of their active halogenating agents, and are further subdivided based on the nature of their mechanism, co-factor, and substrate, as represented in Table 1. Thus, there are three haloperoxidase-types that react through electrophilic mechanisms, namely the heme-, vanadium-, and flavin-dependent haloperoxidases. The *S*-adenosyl-L-methionine (SAM) fluorinases react via nucleophilic pathways, while the nonheme iron/ α -ketoglutarate (α KG)-dependent halogenases react via radical pathways. In the next few sections, we will give a brief overview of these individual halogenases/haloperoxidases and how they differ in their active site structures and reactivities.

Table 1. Classification of the halogenases according to the nature of their active halogenating agent.

Electrophilic	Nucleophilic	Radical
Heme-dependent Vanadium-dependent Flavin-dependent	SAM fluorinases	Nonheme iron/ α KG-dependent halogenase

1.1.1. Heme Haloperoxidases

The first heme-dependent haloperoxidase was discovered from *Caldariomyce fumago* in 1966, the fungus that synthesizes caldariomycin (Figure 2). The link between this haloperoxidase and the biosynthesis of caldariomycin was made from the observation δ -chlorolevulinic acid from β -ketoacid and chloride. The enzyme shows a versatile catalytic ability, but key functions exist that relate to the oxidation of halide ions (iodide, bromide, and chloride) in the presence of hydrogen peroxide to form hypohalous acids. The latter then react non-specifically with electron-rich substrates such as aromatic rings, through chloride transfer, and hence are called chloroperoxidases (CPO).

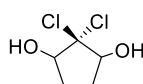


Figure 2. Chemical structure of caldariomycin.

Structurally, CPO shares many of its features with cytochrome P450 enzymes and peroxidases, as outlined with the active site geometries in Figure 3 [16–18]. The P450s are heme monooxygenases that utilize molecular oxygen on a heme center and hydroxylate substrates [19–21]. They tend to bind the heme to the protein via a proximal cysteine ligand, whereas the substrate binds onto the distal site. In heme peroxidases that typically have a histidine proximal ligand, the substrate binding pocket is small and is lined up with polar residues, such as His and Arg amino acids (Figure 3B) [22]. By contrast, on the distal site in CPO, the histidine is missing and its position is taken by a glutamic acid (Glu₁₈₃), while the distal arginine residue in peroxidases is also not present in CPO. An axial cysteinate versus histidine has a profound effect on the chemical properties of the heme as cysteinate

is anionic whereas histidine is neutral. This implies that cysteinate donates electrons to the heme (push-effect), whereas histidine withdraws electron density from the heme [23–27], and consequently CPO/P450 have a much smaller reduction potential than peroxidases and therefore react faster with substrates. Indeed, a series of computational studies on the mechanism and reactivity of P450 versus peroxidases and catalases showed enhanced reactivity of the P450 models [28–33].

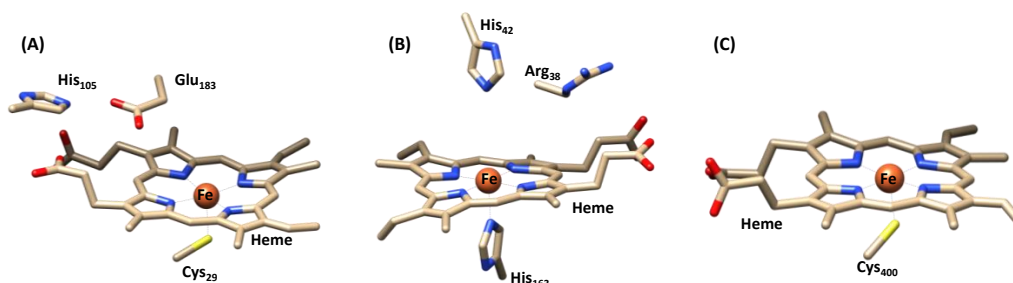


Figure 3. Comparison of the active sites in (A) chloroperoxidase (PDB 1CPO [16]), (B) peroxidase (PDB 2GHC [17]) and (C) cytochrome P450 (PDB 1FAG [18]) enzymes.

The structural differences between CPO, peroxidase, and cytochrome P450 are the result of their functional changes and make CPO specific for chloroperoxidase catalysis. The general mechanism of CPO is shown in Figure 4 and starts from the resting state A, which is a water-bound iron(III)-heme. Upon entering of substrate hydrogen peroxide into the distal binding pocket, water is displaced and transforms structure A to B. Then, Glu₁₈₃ participates in the heterolytic cleavage of the peroxide O–O bond to form the reactive intermediate, Compound I (C) by protonation of the hydroperoxo intermediate, Fe(III)-OOH. The latter is termed Compound 0, and has been studied extensively using various computational models [22,34–40]. Interestingly, mutation of the glutamic acid residue to a histidine greatly hampers its halogenation activity [41]. Compound I then oxidizes a halide anion (X^-) to produce the electrophilic hypohalous acid (XOH) (D) which is then released, and with the addition of water the iron(III) resting state is regenerated [42]. Furthermore, CPO is a crucial model for studying the reaction intermediates of P450 enzymes, and many of the short-lived intermediates of CPO have been characterized by a wide range of spectroscopic methods.

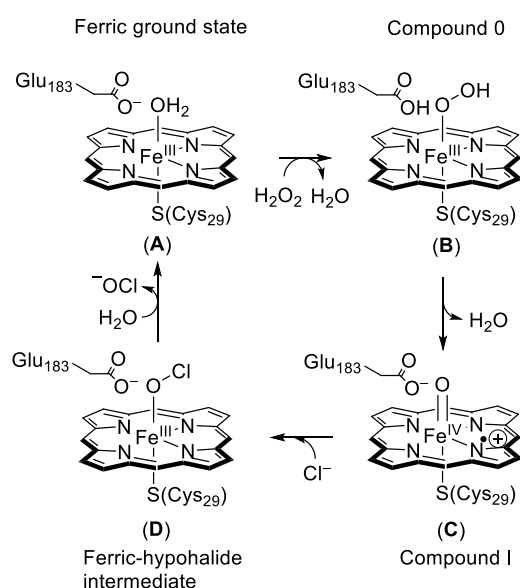


Figure 4. Catalytic cycle of the heme haloperoxidase from chloroperoxidases (CPO). For clarity, the side chains of the heme have been removed.

One of these intermediates is compound I, which has been both spectroscopically characterized [43–45], and studied by computational modelling [46–52]. Furthermore, a variety of spectroscopic techniques have studied short-lived intermediates of CPO through ultraviolet-visible (UV-Vis) absorption [53], resonance Raman [54], electron paramagnetic resonance (EPR) [55,56], and Mössbauer [55] spectroscopic measurements. At the same time, computational studies using density functional theory (DFT) as well as quantum mechanics/molecular mechanics (QM/MM) has given insight into the structure and activity of Compound I [38,50–52,57–60]. Thus, Compound I of CPO reacts with halide anions, typically Cl^- or Br^- , to form hypohalous products in a one-step reaction mechanism [61,62].

In general, heme haloperoxidases activate a broad range of substrates, albeit often unselectively [12,16,63,64] and, therefore, the hypohalous acid is thought to freely diffuse into solution where it reacts with substrates with little selectivity. Currently, there are very few industrial applications of haloperoxidases, due to their low selectivity and stability. In addition, few biomimetic models of halogenases and haloperoxidases have been reported [65–69].

1.1.2. Vanadium Haloperoxidases

Vanadium is the second most common transition metal found in the ocean (after molybdenum), and is usually solvated as vanadate oxyanion at pH 7 [70–72]. Surprisingly, there are only two known enzymes that use vanadium as a co-factor; namely, nitrogenases and vanadium haloperoxidases (V-HPO) [73]. The V-HPOs are found in macroalgae, fungi and bacteria, and are further classified in accordance with the most electronegative halide that they react with. As such, vanadium chloroperoxidases (V-ClPO) can react with chloride, bromide, and iodide, whereas vanadium bromoperoxidases (V-BrPO) react with bromide and iodide only. Finally, the iodoperoxidases (V-IPO) react with iodide alone [74–76]. Together, they exhibit a variety of biological functions and, for example, synthesize several secondary metabolites [77,78] such as sesterterpenes. In addition, neomangicols A–C isolated from the marine fungus *Fusarium* are biosynthesized by V-HPOs. Neomangicols A and B have been shown to display cytotoxic effects toward the HCT-116 human colon tumor cell-line in vitro [79]. Furthermore, in algae, they disrupt bacterial quorum sensing [80], and fungi use them to degrade plant cell walls [81].

The V-HPOs have an activity that is similar to the CPOs mentioned in Section 1.1.1, namely they convert a halide anion to a hypohalous acid. This then reacts as an electrophilic intermediate with electron rich substrates. However, the main difference between the V-HPOs and CPOs is that the oxidation state of vanadium does not change during the catalytic cycle. Therefore, it is not possible for V-HPOs to suffer from oxidative inactivation [2,82–84]. As such the V-HPOs are of great interest from the pharmaceutical industry as potential sources for the synthesis of halogenating compounds. The V-HPOs are also known for their tolerance to organic solvents and resistance against high temperature [85,86] and their ability to oxidize organic sulfides in the absence of halides [87,88]. Furthermore, V-HPOs are thought to be similar to CPO with regards to their low regio- and stereoselectivity. However, two recently discovered V-HPOs show high selectivity in halogenation of their indole substrates [73,89].

Currently, there are crystal structure coordinates from three V-HPOs, namely a V-ClPO from the fungus *C. inaequalis* [76,90,91], V-BrPO from the brown alga *A. nodosum* [92] and V-BrPO from the red alga *C. officinalis* [93]. Despite the fact that the various V-HPO structures share less than a 30% sequence similarity, they all have a common active site structure consisting of two side-by-side four- α -helix bundles with the vanadium core located at the bottom, see Figure 5 [90,92–94]. In addition, they all have an identical arrangement of amino acid residues in the active site, whereby the vanadate oxyanion cofactor is ligated to a histidine residue at the bottom of the four- α -helix bundle that anchors it to the protein [90,92,93].

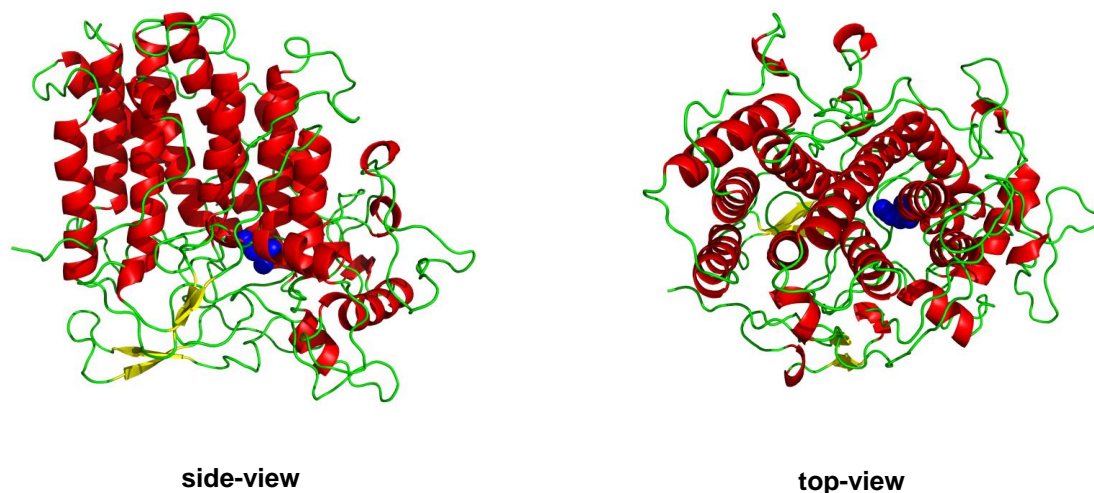


Figure 5. Crystal structure of the vanadium chloroperoxidase from *C. inaequalis* (PDB 1VNC) where we highlight the side-by-side four α -helix loops common to all vanadium haloperoxidases. The vanadium cofactor (blue) is anchored at the bottom of this channel. The structure is shown in the cartoon representation with the secondary structure highlighted; red are α -helices, green are loops, and yellow are β -sheets.

There is still debate about the catalytic mechanism of vanadium haloperoxidases, with questions relating to the nature of the resting state, possible intermediates, and how the co-factor is regenerated. However, computational and experimental studies (mutational and steady state kinetics) on the V-CIPO from *C. inaequalis* have proposed a catalytic mechanism, as shown in Figure 6 [91,93,95–106]. The resting state is thought to be vanadium(V)-dioxo-dihydroxo with one oxo group equatorial and one hydroxo group axial that hydrogen bonds to a protonated histidine residue (His₄₀₄). Research has suggested that as hydrogen peroxide binds, a series of proton transfers occur involving this histidine residue, resulting in the release of water and the generation of vanadium(V)-peroxo(oxo)-hydroxo intermediate [107]. Once the peroxide binds side-on, the vanadium site is distorted from a trigonal bipyramidal to tetragonal bipyramidal [91]. His₄₀₄ then loses its hydrogen bonding interactions to oxygen substituents of vanadium, and instead, Lys₁₅₃ makes direct contact with one of the peroxide oxygen atoms. This is believed to activate the bound peroxide further through charge separation. The vanadium(V)-peroxo(oxo)-hydroxo intermediate then picks up a halide anion to form a vanadium(V)-hypohalide-dioxo(hydroxo) complex. The latter reacts with substrates containing functional groups such as hydrocarbons, sulfides, and olefins. Finally, restoration of the cofactor to its initial resting state is thought to occur again after a series of protonation steps, enabling the hypohalide to leave the active site as hypohalous acid [95].

1.1.3. Flavin Adenine Dinucleotide Haloperoxidases

The flavin adenine dinucleotide (FAD) haloperoxidases were discovered in the 1990s, and were the first halogenases thought to be involved in the regioselective and stereoselective synthesis of halogenated natural products [108]. For example, the first FAD-haloperoxidase was discovered from the biosynthetic gene cluster, responsible for the generation of 7-chlorotetracycline [108]. Subsequently, the enzyme was expressed and characterized both structurally and biochemically [109–122]. Further studies on this group of enzymes has revealed two FAD-haloperoxidase sub-groups, namely those that work on free substrates and ones where the substrate is tethered to a thiolate domain of a non-ribosomal polypeptide synthase system [121]. Despite these differences, they both require reduced flavin (FADH₂) to activate molecular oxygen and to generate C4a-hydroperoxy flavin.

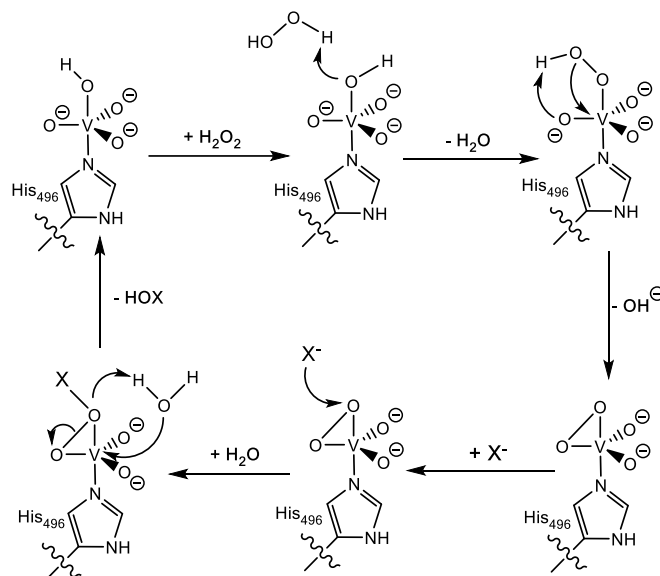


Figure 6. Proposed catalytic cycle of V-XPO.

Originally, the FAD halogenase mechanism was thought to resemble the mechanism of FAD mono-oxygenases; however, structural and biochemical studies in PrnA, a tryptophan halogenase, have proven that this was not the case [110,123]. These studies identified that the substrate binding pocket and flavin binding pocket were 10 Å apart and that the C4a-hydroperoxy flavin was generated before halogenation and in the absence of substrate. Furthermore, the research identified a long-lived enzyme-chloride adduct that was proposed to be a covalent chloramine adduct or a hydrogen bonded lysine-hypochlorous acid species, after identifying that a conserved lysine residue in the active site was highly important.

1.1.4. S-Adenosyl-L-Methionine Fluorinase

All of the halogenases described above in Section 1.1.1, Section 1.1.2, and Section 1.1.3, can use chloride, bromide, and iodide; however, none of those can actually use fluoride. The reasons for this are due to the low bioavailability of fluoride, its high oxidative potential and toxicity. Moreover, because of the high electronegativity of fluoride, it binds polar solvent molecules, such as water, very strongly, which makes it difficult to desolvate fluoride prior to catalysis [2]. Surprisingly, one class of halogenases, namely F1A from *Streptomyces cattleya*, is able to fluorinate substrates using an S-adenosyl-L-methionine (SAM) co-factor to 5'-fluorodeoxyadenosine and L-methionine via a nucleophilic substitution [124,125]. Since then, genome mining has discovered several other SAM fluorinases [126] and further study has elucidated part of its mechanism.

Computational and structural studies [127,128] revealed that conformational changes in the protein upon binding fluoride and SAM are important for reactivity. As such, lining the fluoride binding pocket is charged residues which upon fluoride binding help with the assistance of others to exclude the majority of the water from the active site, thereby, increasing the nucleophilicity of fluoride.

1.1.5. Nonheme Iron/ α -Ketoglutarate Halogenases

The investigation into the synthesis of barbamide, a trichlorinated compound, from the marine cyanobacterium *Lyngbya majuscula*, led to the conclusion that there was another class of halogenases not yet catalogued which could regioselectively and stereospecifically halogenate a substrate other than the FAD halogenases [63]. Further investigation identified that they required iron(II), molecular oxygen, α -ketoglutarate (α KG), a halogen (chloride or bromide) and an aliphatic substrate. These enzymes were found to be similar in structure to the nonheme iron/ α KG dependent hydroxylases

(NHFeHy), and therefore, were named the nonheme iron/ α KG dependent halogenases (NHFeHa). So far, seven known NHFeHa proteins have been identified and characterized, namely BarB1, BarB2, SyrB2, CytC3, CmaB, HctB, and WelO5. Although most of these proteins show considerable differences in structure and reactivity all efficiently activate aliphatic substrates and convert a C–H bond to a C–X (X = Br, Cl) bond. Of the set of NHFeHas, the most extensively studied one is SyrB2 because it was the first to be purified for biochemical characterization [2].

Common to all NHFeHas and NHFeHys is the 8-stranded anti-parallel β -jelly roll motif which binds the iron necessary for the catalytic activity to occur through the facial triad residues consisting of Asp(Glu)/His/His in NHFeHys and His/His in NHFeHas. Figure 7 highlights the comparisons and differences of the tertiary protein structure in NHFeHy and NHFeHa enzymes. As can be clearly seen from A-1 and B-1 the fold is very similar with helices in almost the same position. A close up of the active site with its environment is then compared in parts A-2 and B-2 in Figure 7, which shows almost identical protein active site structure. In the final parts (A-3 and B-3) the metal coordination is highlighted that has the typical 2-His/1-Asp in the hydroxylases and the 2-His/1-Cl binding pattern in halogenases. In NHFeHas the aspartate/glutamate residue is substituted for an alanine which creates space for halide to coordinate to the iron [127] (Figure 7). There are several NHFeHy enzymes; however, that bind the metal through three histidine residues. Most of these enzymes are associated with cysteine binding and catalysis. For instance, cysteine dioxygenase binds cysteine and converts it into cysteine sulfinic acid on a NHFeHy active site with three facial His residues [129–133]. Another NHFeHy with a 3-His ligand coordination is the sulfoxide synthase enzyme EgtB that is involved in the biosynthesis of ergothioneine [134].

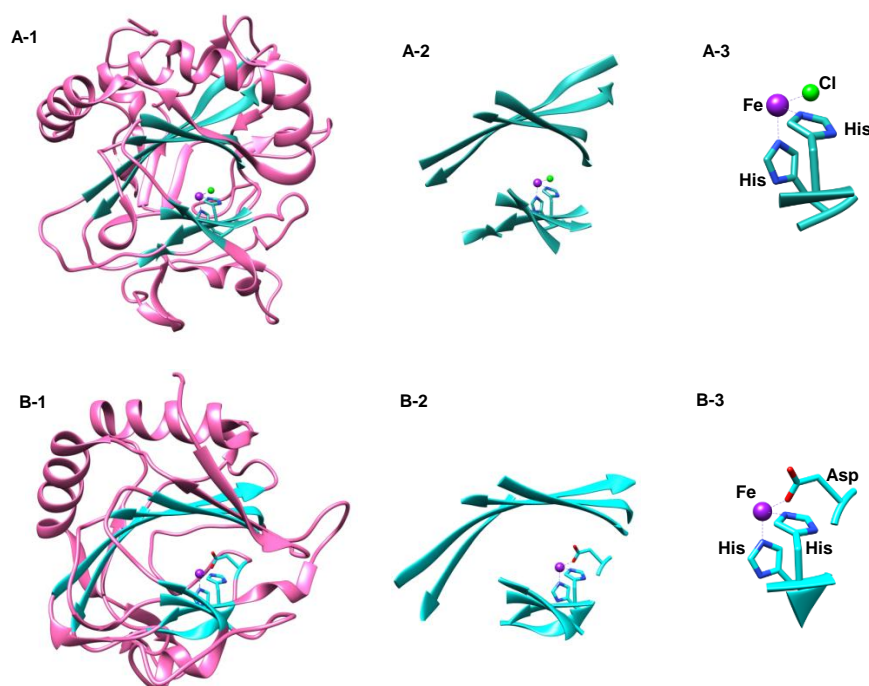


Figure 7. Basic components and comparison between the nonheme iron halogenase, SyrB2 (A) from *Pseudomonas syringae* (PDB 2FCT) and the nonheme iron hydroxylase, prolyl-4-hydroxylase (B) from *Clamydomonas reinhardtii* (PDB 2JIG). A-1 & B-1 show similarities in tertiary structure. A-2 & B-2 show the similarities in each 8-stranded anti-parallel β -Jelly roll motif common to most nonheme iron enzymes. A-3 shows the facial triad typical of halogenases in contrast to B-3 showing the facial triad typical of hydroxylases.

Originally, substituting the aspartate/glutamate in NHFeHys by glycine was thought to be the governing reason defining halogenation. However, recent studies on active site mutants of

both NHFeHas and NHFeHys failed to convert the halogenase into a hydroxylase and vice versa. Therefore, the reasons governing the catalytic difference of halogenases versus hydroxylases are more complex than first thought [64,127,135] and have triggered further detailed mechanistic computational and experimental work. Specifically, most NHFeHas require their substrate be tethered to a phosphopantetheine arm (PPT) associated with an acyl-carrier protein (ACP) [136,137], whereas the hydroxylases tend to have free substrates, although they are often bound tightly in a substrate binding pocket. For example, the prolyl-4-hydroxylase from *Clamydomonas reinhardtii* tightly binds the substrate through selective hydrogen bonding involving amino acids in two loops (β_3 - β_4 loop and the β_{II} - β_{III}) which cover the substrate [138,139]. The only halogenase that forms an exception to this rule appears to be WelO5, whose recent discovery revealed that it did not require a PPT arm to deliver its substrate into the active site. Instead, it uses a free substrate, 12-epi-fischerindole U [140–142]. The variation in substrate scope and the ability to introduce a halogen to an aliphatic carbon make the NHFeHas desirable biotechnological targets, and thus their mechanism and reasons governing halogenation vs. hydroxylation must be understood.

The catalytic cycle of nonheme iron halogenases is split into two parts: the generation of the iron(IV)-oxo oxidant and the production of the halogenated product as shown in Figure 8. The catalytic cycles of NHFeHa and NHFeHy are identical from the resting state unto the formation of the iron(III)-hydroxo complex **G**, but bifurcate thereafter [143–154]. The cycle starts from the resting state (**A**) that consists of an iron(II) atom bound to three water molecules, and which is linked to the protein via two His residues. The final coordination site on the iron is occupied by a carboxylate of an Asp/Glu residue in NHFeHys, but a halide is present in the NHFeHas. With the addition of α KG, two water molecules are displaced and α KG binds to iron as a bidentate ligand (**B**). As the substrate binds into the enzyme, it does not coordinate to iron(II) directly, but displaces the last water ligand (**C**), and molecular oxygen fills its position, thereby forming the iron(III)-superoxo species (**D**). The terminal oxygen atom of superoxo then attacks α KG at the nucleophilic carbon atom of the keto moiety producing a peroxy-succinate bicyclic ring intermediate (**E**). As the reaction proceeds, this bicyclic ring structure decomposes, producing the iron(IV)-oxo, succinate and carbon dioxide (**F**). The iron(IV)-oxo has been spectroscopically characterized and is a powerful oxidant in NHFe enzymes. In NHFeHys and NHFeHas the iron(IV)-oxo performs a rate-determining hydrogen atom abstraction reaction from bound substrate producing iron(III)-hydroxy(halide) and a radical on the substrate (**G**) [155,156]. At this point, the reaction mechanism bifurcates, and the chloride radical species rebounds to the radical substrate forming the final halogenated product in the halogenases, whereas OH rebound gives alcohol products for the hydroxylases. Restoration to the resting state (**A**) in halogenases occurs when three water molecules displace the hydroxyl group and succinate bound to iron, and an additional chloride atom binds; however, these steps are yet to be eluded [157–159].

Computational and experimental studies of biological and biomimetic systems have helped to elucidate this general mechanism [143–154]. However, variations in biological systems are being identified, which are helping to shed further light on the differences and factors relating to the bifurcation of these systems, leading to either halogenated or hydroxylated products. Some of the differences between halogenases and hydroxylases relate to the generation of the iron(IV)-oxo oxidant and how the products are formed, which will be discussed in more detail in the following sections.

Due to the nature of the short-lived intermediates formed in the generation of the iron(IV)-oxo, their observation using experimental techniques is challenging. Therefore, computational methods have been at the heart of understanding these steps. Much of the work has focused on NHFeHys [103,145,148,158–167]; however, the mechanism is believed to be similar in the NHFeHas [168,169]. Results from six computational studies have suggested various additional intermediates for the mechanism linked to the production of the iron(IV)-oxo [169–174]. As mentioned above, the catalytic cycle of NHFeHys and NHFeHas is largely similar; however, post-hydrogen atom abstraction from the substrate, the systems bifurcate. In the NHFeHys, a hydroxyl radical rebounds, forming the hydroxylated product [138,139,148,149], in contrast to NHFeHas, whereby, a chloride

radical relay gives the halogenated product. The factors related to bifurcation have been the subject of study for many years, ever since the discovery of NHFeHas, and has created a number of controversies and mechanistic possibilities. Thus, the origin of the substrate halogenation pathway were found to be dependent on: (i) substrate placement [168–171], (ii) protonation of the axial Fe(III)-OH post hydrogen abstraction [172], (iii) the bond dissociation energy of chloride vs. hydroxyl [173], (iv) reaction of liberated CO₂ from α KG with Fe(III)-OH [174], (v) the reduction potential of chloride vs. hydroxyl [175], (vi) concomitant hydrogen atom transfer and radical chlorination [173], (vii) isomerization of the Cl-Fe(IV)=O intermediate [176], (viii) isomerization of the Cl-Fe(III)-OH [177] and (ix) the perturbations of the protein [177,178].

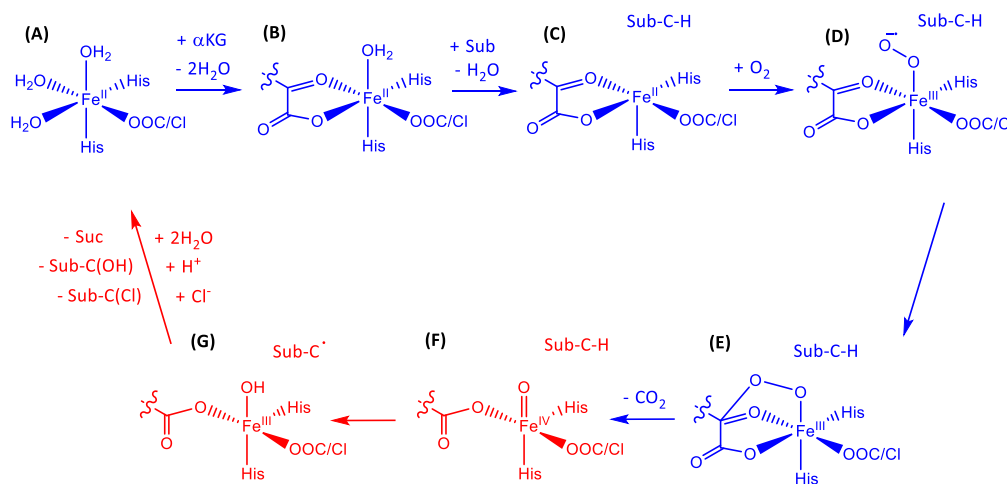


Figure 8. Catalytic mechanism of nonheme iron halogenases and hydroxylases.

The positioning of the substrate relative to the iron(IV)-oxo has gained the most theoretical and experimental support [168–171,178]; however, it may not be the sole factor responsible, but rather a combination of factors. Nevertheless, the substrate placement hypothesis states that the substrate C–H bond must be held away from the iron(IV)-oxo, with bond vectors close the perpendicular, thereby directing hydrogen atom abstraction through the π -pathway [179]. Most NHFeHas have their substrate attached to a PPT arm which is tethered to an acyl carrier protein (ACP) [180,181], and all three are required for proper activation of the enzyme. Interestingly, WelO5 binds its substrate in the absence of this extra machinery [140–142]. In a study on NHFeHas the effects of substrate placement on product outcome is difficult as no crystal structure has been resolved yet with substrate bound (not including WelO5). Several spectroscopic techniques and computational methods were used with deuterium-labeled substrates that have given insight into substrate positioning and reactivity patterns.

2. Computational Studies on Nonheme Iron Hydroxylases and Halogenases

In this section, some examples of recent studies of our group are presented, which have focused on the mechanistic features of nonheme iron halogenases and hydroxylases. Thus, both NHFeHa and NHFeHy have a catalytic cycle similar to the one in Figure 8, which starts from a resting state A. After the substrate, α -ketoglutarate and dioxygen binding is converted into an iron(IV)-oxo species (F). The latter abstracts a hydrogen atom from substrate to form an iron(III)-hydroxo species and a substrate radical. From that point onwards, there are different pathways for halogenases and hydroxylases, Figure 9. Thus, the halogenases rebound the halide atom to form halogenated substrate, whereas the hydroxylases form alcohol products.

In the next few sections, examples of computational studies on nonheme iron halogenases and hydroxylases from our group will be presented. In particular, a recent extensive QM/MM study on the hectochlorin biosynthesis enzyme (HctB) [178] established insight into the effect of the protein on the

bifurcation pathways leading to halogenation and hydroxylation (Section 2.1). In Section 2.2 we will review recent work on the nonheme iron hydroxylase prolyl-4-hydroxylase (P4H), which is involved in the biosynthesis of 4-hydroxy-proline in the body. These studies use computational modelling and particularly focus on the QM/MM technique, which we will describe briefly first.

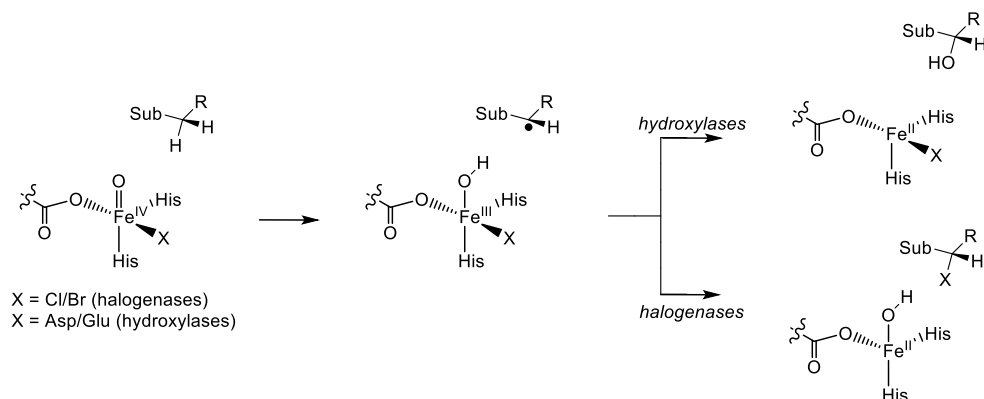


Figure 9. Catalytic mechanism of substrate halogenation versus hydroxylation of substrate by NHFeHa and NHFeHy enzymes.

The QM/MM method considers a complete enzyme that is fully solvated and contains a substrate, a co-factor, co-substrates, and counter ions [182]. These chemical systems, therefore, mimic the environment of the real system and often put restrictions on the mobility of the substrate in the pocket. QM/MM studies, in contrast to small model complexes, therefore, often reproduce experimental regio- and stereoselectivities and product distributions as a result of substrate positioning and the interactions of the protein [182–186].

In QM/MM, the computational model set up usually starts from crystal structure coordinates, which are then modified to the required starting position. For instance, a resting state enzyme is converted into the active site structure manually. In some cases, a substrate is missing that will need to be docked in, or mutations need to be undone. Finally, some crystal structure coordinates have chains, co-factors or amino acids missing that will need to be inserted as well. After these initial corrections and modifications, hydrogen atoms are added, which is not a straightforward process, as some amino acid residues are weak acids and are in present different protonation states depending on their environment. Key amino acid residues, such as histidine groups will need to be visually checked for their correct protonation state assignment. In the final stage of the set-up, solvent (water) is added by fixing the protein. This can be done iteratively to enable the solvent to enter the protein. After the model is completed a molecular dynamics simulation is run for a minimum of 1000 ps at room temperature conditions. From the relaxed simulation part, some low energy structures (snapshots) are selected for the actual QM/MM calculations.

In QM/MM, the inner region of the protein—i.e., the active site with substrate and key residues—is calculated with QM or DFT methods, whereas the rest of the protein is calculated with cheap MM methods. This enables studies on full proteins that keep the orientation and constraints of the enzyme in the model. These studies are reasonably accurate, and recent benchmark and calibration studies that compare a range of density functional theory methods versus experimental rate constants, kinetic isotope effects, and spectroscopic parameters are in good agreement [187–193].

2.1. Hectochlorin Biosynthesis Enzyme

Early density functional theory calculations of our group [174] showed that the hydrogen atom abstraction is the rate-determining step, leading to an iron(III)-hydroxo(chloride) complex that can either do hydroxo or chloride rebound to form products. For small model complexes the barriers for OH rebound were found to be substantially smaller than those for halide transfer in contrast

to experimental observation. Therefore, a detailed QM/MM study was performed [178]. In this particular case, a model of the hectochlorin biosynthesis enzyme (HctB) that generated a nonheme iron(IV)-oxo(chloride) species (the reactant Re) was investigated (Figure 10). It is linked to the protein through two histidine amino acids and also binds succinate. The substrate is a fatty-acyl tethered substrate linked to an acyl-carrier domain.

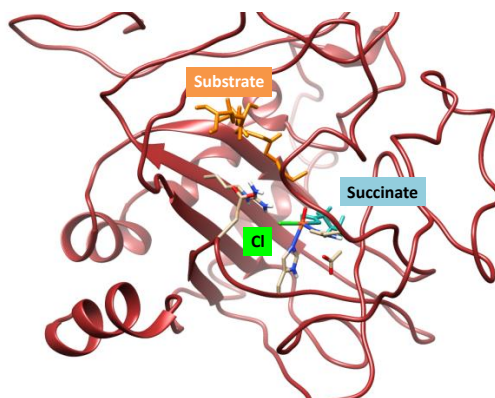


Figure 10. Protein structure of the halogenase domain of HctB with substrate, chloride, and succinate bound. Protein strands in wine-red, chloride in green, succinate in light blue, iron in amber, and oxo group in red.

Subsequently, we investigated substrate halogenation and hydroxylation from the model in Figure 10 using QM/MM, and the obtained halogenation and hydroxylation mechanism of the (ω -1)-position of substrate is shown in Figure 11. In principle, we tested the mechanism on four low-lying spin states (singlet, triplet, quintet, and sextet), but the quintet was considerably lower in energy than the other spin states, and hence we will focus on the quintet spin results only. As the spin-state ordering of iron complexes is sometimes dependent on the density functional method and on the fact that B3LYP tends to overstabilize high-spin states [194], we tested alternative density functional methods as well. The spin state ordering is the same regardless of the density functional method chosen for the calculations, and shows little variation. We initially did a geometry optimization of the reactant complexes after a detailed set-up that included a 10 ns molecular dynamics simulation.

The reaction is stepwise, starting with a hydrogen atom abstraction leading to an iron(III)-hydroxo(chloro) intermediate ($^5\text{I}_{\text{HA}}$) via a hydrogen atom abstraction barrier ($^5\text{TS}_{\text{HA}}$). Subsequently, either chloro rebinds via $^5\text{TS}_{\text{Cl}}$ leads to chlorinated products ($^5\text{P}_{\text{Cl}}$), or hydroxo rebinds via $^5\text{TS}_{\text{OH}}$ to form hydroxylated products ($^5\text{P}_{\text{OH}}$). As such the reaction, is stepwise via a radical intermediate. This mechanism is reminiscent of substrate hydroxylation that often shows a rate-determining hydrogen atom abstraction via a radical intermediate [195–204]. Initially, a number of geometry scans were performed for the hydrogen atom abstraction pathways, which gave us starting points for the hydrogen atom abstraction transition states. The hydrogen atom abstraction is rate-determining with a barrier of $\Delta E + \text{ZPE} = 20.8 \text{ kcal mol}^{-1}$ on the quintet spin state surface. Consequently, the lifetime of the intermediate ($^5\text{I}_{\text{HA}}$) will be dependent on the subsequent barrier leading to products. The hydrogen atom abstraction transition state (Figure 11) has a relatively long O–H bond of 1.452 Å and a somewhat shorter C–H distance of 1.221 Å. Often, these types of reactant-like transition states with shorter C–H than O–H distances, correspond to higher barriers than product-like transition states [195,205]. The imaginary frequency in the transition state is relatively low ($i551 \text{ cm}^{-1}$), although it still should lead to a significant kinetic isotope effect upon replacement of the transferring hydrogen atom by deuterium [206–208].

Previously, using small model complexes, we found that the substrate hydroxylation pathway is more exothermic and has smaller barriers than the halogenation pathway [66,174]. As such, the protein affects the mechanism of the reaction dramatically and drives the reaction toward the unfavorable

halogenation pathway. Clearly, the protein environment positions the substrate in the ideal orientation for halide transfer. This comes at a cost, as the hydrogen atom abstraction is relatively high in energy. Consequently, substrate positioning makes hydrogen atom abstraction more difficult, but prevents direct OH rebound and enables halogen rebound instead.

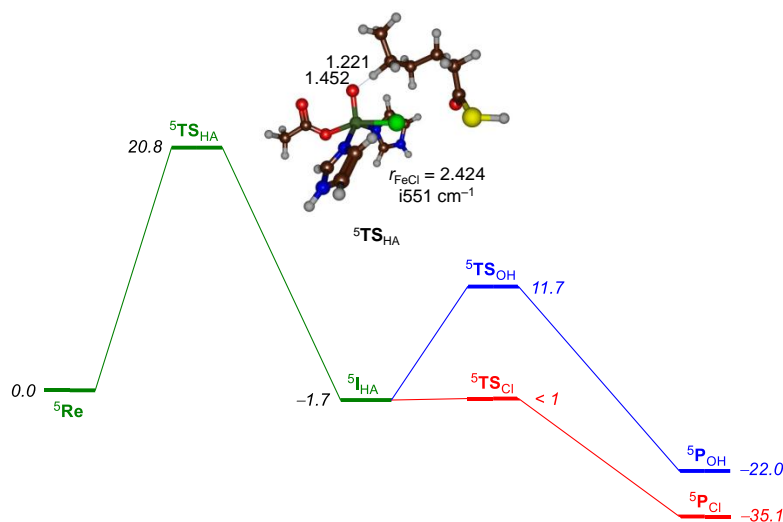


Figure 11. Quantum mechanics/molecular mechanics (QM/MM)-calculated reaction mechanism of substrate chlorination and hydroxylation by an iron(IV)-oxo oxidant in HctB. Energies (in kcal mol⁻¹) obtained at UB3LYP/SV(P) with zero-point corrections included. Hydrogen atom abstraction transition state with bond lengths in angstroms and the imaginary frequency in wave numbers.

To understand the origin of the selectivity of the reaction, we did a detailed analysis of the protein structure as compared to small active site models in the gas-phase. Figure 12 shows the QM/MM-optimized geometry of the reactant complex, i.e., iron(IV)-oxo(chloride). The metal is in pentacoordination with the oxo-group trans to His₂₂₇, whereas the chloride is in the equatorial plane together with the carboxylate of succinate and His₁₁₁. Interestingly, on the same line as the Fe-Cl axis, we find the carboxylate of Glu₂₂₃. This implies that the negative charge from Glu₂₂₃ will push electron density away from the chloride group towards the iron and make the halide less anionic. The charge-donation of Glu₂₂₃ will make the halide lesser anionic, i.e., more radicalar, and hence easier to transfer to substrates than the corresponding anion. Furthermore, the substrate is positioned in a corner of the protein near to the halide. It appears, therefore, that nonheme iron halogenases have an intricately designed structure where the oxidant and substrate are positioned in such a way that a thermodynamically unfavorable reaction pathway can proceed.

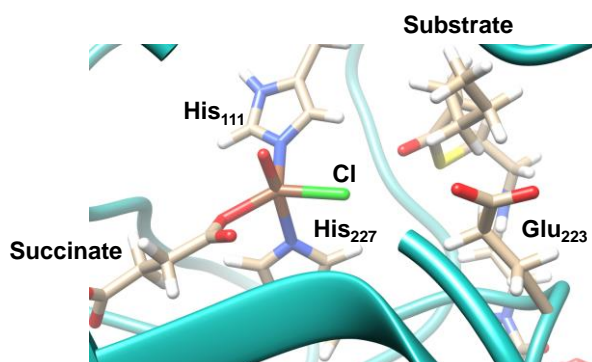


Figure 12. QM/MM-optimized geometry (B3LYP/SV(P):Charmm) of the iron(IV)-oxo(chloride) reactant complex. Key amino acids and functional groups highlighted.

2.2. Prolyl-4-Hydroxylase

Prolyl-4-hydroxylase is a nonheme iron hydroxylase with importance for human health as it is involved in the biosynthesis of *R*-4-hydroxyproline, an essential element in the collagen crosslinking process in the body. This reaction is stereo- and regiospecific, and moreover, a thermodynamically unfavorable reaction is catalyzed [149]. Thus, studies of small model complexes showed that it is easier to hydroxylate the C⁵ position of proline than C⁴ position. Therefore, a QM/MM study [138,139] was performed to establish the protein involvement in the reaction mechanism. The main results are shown in Figure 13. Thus, the reaction is stepwise starting from an iron(IV)-oxo intermediate (**Re**) in the quintet spin ground state. Subsequently, a hydrogen atom abstraction transition state (**TS_H**) leads to an iron(III)-hydroxo intermediate (**I_H**) and a final rebound transition state (**TS_{reb}**) results in alcohol products (**P**).

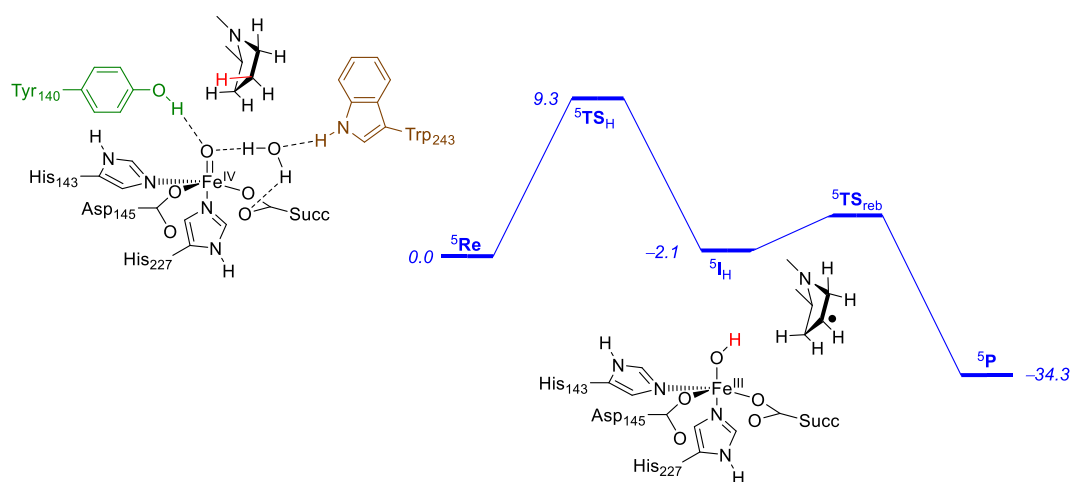


Figure 13. QM/MM-optimized potential energy landscape (UB3LYP/SV(P):Charmm) for proline hydroxylation at the C⁴-position. Energies contain zero-point corrections and are in kcal mol⁻¹. Key amino acids and functional groups highlighted.

The hydrogen atom abstraction has a barrier of 9.3 kcal mol⁻¹ and is rate-determining. Interestingly, we find a 1 kcal mol⁻¹ higher barrier for hydrogen atom abstraction from the C⁵ position of proline [138], even though this should be thermodynamically easier. Hydrogen atom abstraction from the other positions at C⁴ and C⁵, as well as from C³ (both positions) were studied as well, and found to be considerably higher in energy. Therefore, prolyl-4-hydroxylase reacts with proline residues stereo- and regioselectively and will give dominant *R*-4-hydroxyproline as products. Clearly, the protein is designed in such a way for perfect fit of oxidant with substrate so that only the 4-position of substrate can be activated.

Note that in the reactant complex (structure in Figure 13) the iron(IV)-oxo group is stabilized through hydrogen bonding interactions of the phenol group of Tyr₁₄₀, and also via a water molecule to the indole group of Trp₂₄₃. As such, the active site will be very rigid. Furthermore, the substrate is also in a tight orientation and is locked by the aromatic rings of Tyr₁₄₀ and Trp₂₄₃, but is also held in position through hydrogen bonding interactions along the chain with, for instance, Glu₁₂₇ and Arg₁₆₁. Active site mutations that replaced Arg₁₆₁ with either Asp or Lys led to complete inactivity of the protein. A similar effect was seen for the mutation of Glu₁₂₇ with Lys. Mutations of Tyr₁₄₀ and Trp₂₄₃ by either Phe or Gly led to loss of selectivity or complete loss of activity. Therefore, prolyl-4-hydroxylase has a tightly controlled substrate and an oxidant binding orientation that enables close contact between the oxidant and substrate at the C⁴ position. Disruption of the substrate binding position and orientation leads to major shifts in the position of the substrate and its activation. Indeed, we tested several active

site mutants, where, e.g., Trp₁₄₀ and Trp₂₄₃ were replaced by smaller residues. In all cases, loss of stereo- and regioselectivity was observed, and in most of them, a complete loss of activity was found.

3. Conclusions

This paper reviews enzymatic halogenases and haloperoxidases, which comes in a range of structural forms. Thus, haloperoxidases utilize dioxygen on a co-factor active site, and using a halide anion ($\text{Cl}^-/\text{Br}^-/\text{I}^-$), produce hypohalide anions ($\text{OCl}^-/\text{OBr}^-/\text{OI}^-$) that transfer their halide to substrates. The haloperoxidases come in three different forms, namely the heme-iron-dependent, vanadium-dependent, and flavin-dependent structures that catalyze the same reaction but utilize a different co-factor. Halogenases typically have a nonheme iron active site that is structurally and functionally analogous to the nonheme iron hydroxylases, and bind the metal to two histidine amino acids of the protein. In addition, the hydroxylases have a carboxylate of either Glu or Asp linked to the iron co-factor, whereas in the halogenases, that position is occupied by a halogen. Both nonheme iron halogenases and hydroxylases bind α -ketoglutarate and molecular oxygen on the iron(II) center and form succinate, a nonheme iron(IV)-oxo species and CO_2 . Thereafter, they react via an aliphatic hydrogen atom abstraction to form iron(III)-hydroxo and a substrate radical that recombines to form the alcohol product in the hydroxylases. By contrast, in the halogenases, this step is prevented and a halogen rebound takes place. How proteins manage to bypass thermodynamically favorable pathways to catalyze a regio- and chemoselective reaction mechanisms is still under discussion, and computational modelling can give insights into the pathways leading to products and by-products. Examples are discussed on the origin of the regio- and chemoselectivity of the hectochlorin biosynthesis enzyme in enzymatic halogenation, and prolyl-4-hydroxylase for stereoselective hydroxylation.

Author Contributions: A.T. and S.P.d.V. wrote the paper.

Acknowledgments: We acknowledge the BBSRC (Biotechnology and Biological Sciences Research Council UK) for a studentship of a studentship under grant code BB/J014478/1.

Conflicts of Interest: The authors declare no conflict of interest. The founding sponsors had no role in the design of the study; in the collection, analyses, or interpretation of data; in the writing of the manuscript, and in the decision to publish the results.

References

1. Gribble, G.W. The diversity of naturally produced organohalogenes. *Chemosphere* **2003**, *52*, 289–297. [[CrossRef](#)]
2. Vaillancourt, F.H.; Yeh, E.; Vosburg, D.A.; Garneau-Tsodikova, S.; Walsh, C.T. Nature's inventory of halogenation catalysts: Oxidative strategies predominate. *Chem. Rev.* **2006**, *106*, 3364–3378. [[CrossRef](#)] [[PubMed](#)]
3. Cabrita, M.T.; Vale, C.; Rauter, A.P. Halogenated compounds from marine algae. *Mar. Drugs* **2010**, *8*, 2301–2317. [[CrossRef](#)] [[PubMed](#)]
4. Van Pee, K.-H. Biosynthesis of halogenated metabolites by bacteria. *Annu. Rev. Microbiol.* **1996**, *50*, 375–399. [[CrossRef](#)] [[PubMed](#)]
5. Laus, G. Biological activities of natural halogen compounds. *Stud. Nat. Prod. Chem.* **2001**, *25*, 757–809. [[CrossRef](#)]
6. Stonik, V.A.; Fedorov, S.N. Marine low molecular weight natural products as potential cancer preventative compounds. *Mar. Drugs* **2014**, *12*, 636–671. [[CrossRef](#)] [[PubMed](#)]
7. Blunt, J.W.; Copp, B.R.; Hu, W.P.; Munro, M.H.G.; Northcote, P.T.; Prinsep, M.R. Marine natural products. *Nat. Prod. Rep.* **2009**, *26*, 170–244. [[CrossRef](#)] [[PubMed](#)]
8. Jeschke, P. The unique role of fluorine in the design of active ingredients for modern crop protection. *ChemBioChem* **2004**, *5*, 570–589. [[CrossRef](#)] [[PubMed](#)]
9. Jeschke, P. The unique role of halogen substituents in the design of modern agrochemicals. *Pest Manag. Sci.* **2010**, *66*, 10–27. [[CrossRef](#)] [[PubMed](#)]

10. Nakama, Y.; Yoshida, O.; Yoda, M.; Araki, K.; Sawada, Y.; Nakamura, J.; Xu, S.; Miura, K.; Maki, H.; Arimoto, H. Discovery of a novel series of semisynthetic vancomycin derivatives effective against vancomycin-resistant bacteria. *J. Med. Chem.* **2010**, *53*, 2528–2533. [[CrossRef](#)] [[PubMed](#)]
11. Cavallo, G.; Matrangolo, P.; Milani, R.; Pilati, T.; Primagi, A.; Resnati, G.; Tarraneo, G. The halogen bond. *Chem. Rev.* **2016**, *116*, 2478–2601. [[CrossRef](#)] [[PubMed](#)]
12. Lantham, J.; Brandenburger, E.; Shepherd, S.A.; Menon, B.R.K.; Micklefield, J. Development of halogenase enzymes for use in synthesis. *Chem. Rev.* **2017**, *111*, 232–269. [[CrossRef](#)]
13. Tang, M.L.; Bao, Z. Halogenated materials as organic semiconductors. *Chem. Mater.* **2011**, *23*, 446–455. [[CrossRef](#)]
14. Berger, G.; Soubhye, J.; Meyer, F. Halogen bonding in polymer science: From crystal engineering to functional supramolecular polymers and materials. *Polym. Chem.* **2015**, *6*, 3559–3580. [[CrossRef](#)]
15. Amanchukwu, C.V.; Harding, J.R.; Shao-Horn, Y.; Hammond, P.T. Understanding the chemical stability of polymers for lithium-air batteries. *Chem. Mater.* **2015**, *27*, 550–561. [[CrossRef](#)]
16. Sundaramoorthy, M.; Turner, J.; Poulos, T.L. The crystal structure of chloroperoxidase: A heme-peroxidase-cytochrome P450 functional hybrid. *Structure* **1995**, *3*, 1367–1377. [[CrossRef](#)]
17. Badyal, S.K.; Joyce, M.G.; Sharp, K.H.; Seward, H.E.; Mewies, M.; Basran, J.; Macdonald, I.K.; Moody, P.C.E.; Raven, E.L. Conformational mobility in the active site of the heme peroxidase. *J. Biol. Chem.* **2006**, *281*, 24512–24520. [[CrossRef](#)] [[PubMed](#)]
18. Li, H.; Poulos, T.L. The structure of the cytochrome P450M-3 haem domain complexed with the fatty acid substrate, palmitoleic acid. *Nat. Struct. Mol. Biol.* **1997**, *4*, 140–146. [[CrossRef](#)]
19. Meunier, B.; de Visser, S.P.; Shaik, S. Mechanism of oxidation reactions catalyzed by cytochrome P450 enzymes. *Chem. Rev.* **2004**, *104*, 3947–3980. [[CrossRef](#)] [[PubMed](#)]
20. Denisov, I.G.; Makris, T.M.; Sligar, S.G.; Schlichting, I. Structure and chemistry of cytochrome P450. *Chem. Rev.* **2005**, *105*, 2253–2277. [[CrossRef](#)] [[PubMed](#)]
21. Ortiz de Montellano, P.R. Hydrocarbon hydroxylation by cytochrome P450 enzymes. *Chem. Rev.* **2010**, *110*, 932–948. [[CrossRef](#)] [[PubMed](#)]
22. De Visser, S.P.; Nam, W. High-valent iron-oxo porphyrins in oxygenation reactions. In *Handbook of Porphyrin Science*; Kadish, K.M., Smith, K.M., Guilard, R., Eds.; World Scientific Publishing Co.: Hackensack, NJ, USA, 2010; Chapter 44; pp. 85–140, ISBN-13 978-981-4307-23-9.
23. Ogliaro, F.; de Visser, S.P.; Cohen, S.; Kaneti, J.; Shaik, S. The experimentally elusive oxidant of cytochrome P450: A theoretical “trapping” defining more closely the “real” species. *ChemBioChem* **2001**, *2*, 848–851. [[CrossRef](#)]
24. De Visser, S.P.; Ogliaro, F.; Gross, Z.; Shaik, S. What is the difference between the manganese porphyrin and corrole analogs of cytochrome P450's Compound I? *Chem. Eur. J.* **2001**, *7*, 4954–4960. [[CrossRef](#)]
25. De Visser, S.P.; Shaik, S.; Sharma, P.K.; Kumar, D.; Thiel, W. Active species of horseradish peroxidase (HRP) and cytochrome P450: Two electronic chameleons. *J. Am. Chem. Soc.* **2003**, *125*, 15779–15788. [[CrossRef](#)] [[PubMed](#)]
26. Shaik, S.; de Visser, S.P.; Kumar, D. External electric field will control the selectivity of enzymatic-like bond activations. *J. Am. Chem. Soc.* **2004**, *126*, 11746–11749. [[CrossRef](#)] [[PubMed](#)]
27. De Visser, S.P. What affects the quartet-doublet energy splitting in peroxidase enzymes? *J. Phys. Chem. A* **2005**, *109*, 11050–11057. [[CrossRef](#)] [[PubMed](#)]
28. Kumar, D.; de Visser, S.P.; Sharma, P.K.; Derat, E.; Shaik, S. The intrinsic axial ligand effect on propene oxidation by horseradish peroxidase versus cytochrome P450 enzymes. *J. Biol. Inorg. Chem.* **2005**, *10*, 181–189. [[CrossRef](#)] [[PubMed](#)]
29. Kumar, D.; de Visser, S.P.; Sharma, P.K.; Hirao, H.; Shaik, S. Sulfoxidation mechanisms catalyzed by cytochrome P450 and horseradish peroxidase models: Spin selection induced by the ligand. *Biochemistry* **2005**, *44*, 8148–8158. [[CrossRef](#)] [[PubMed](#)]
30. De Visser, S.P. The axial ligand effect of oxo-iron porphyrin catalysts. How does chloride compare to thiolate? *J. Biol. Inorg. Chem.* **2006**, *11*, 168–178. [[CrossRef](#)] [[PubMed](#)]
31. De Visser, S.P. Can the replacement of a single atom in the enzyme horseradish peroxidase convert it into a monooxygenase? A density functional study. *J. Phys. Chem. B* **2006**, *110*, 20759–20761. [[CrossRef](#)] [[PubMed](#)]
32. Wang, R.; de Visser, S.P. How does the push/pull effect of the axial ligand influence the catalytic properties of Compound I of catalase and cytochrome P450? *J. Inorg. Biochem.* **2007**, *101*, 1464–1472. [[CrossRef](#)] [[PubMed](#)]

33. Kumar, D.; Karamzadeh, B.; Sastry, G.N.; de Visser, S.P. What factors influence the rate constant of substrate epoxidation by Compound I of cytochrome P450 and analogous iron(IV)-oxo oxidants. *J. Am. Chem. Soc.* **2010**, *132*, 7656–7667. [[CrossRef](#)] [[PubMed](#)]
34. Silaghi-Dumitrescu, R. Halide activation by heme peroxidases: Theoretical predictions on putative adducts of halides with Compound I. *Eur. J. Inorg. Chem.* **2008**, *2008*, 5404–5407. [[CrossRef](#)]
35. Ogliaro, F.; de Visser, S.P.; Cohen, S.; Sharma, P.K.; Shaik, S. Searching for the second oxidant in the catalytic cycle of cytochrome P450: A theoretical investigation of the iron(III)-hydroperoxo species and its epoxidation pathways. *J. Am. Chem. Soc.* **2002**, *124*, 2806–2817. [[CrossRef](#)] [[PubMed](#)]
36. Sharma, P.K.; Kevorkiants, R.; de Visser, S.P.; Kumar, D.; Shaik, S. Porphyrin trap its own terminator! Concerted and stepwise porphyrin degradation mechanisms induced by heme-oxygenase vs. cytochrome P450. *Angew. Chem. Int. Ed.* **2004**, *43*, 1129–1132. [[CrossRef](#)] [[PubMed](#)]
37. Kumar, D.; de Visser, S.P.; Shaik, S. Theory favors a stepwise mechanism of porphyrin degradation by a ferric hydroperoxide model of the active species of heme oxygenase. *J. Am. Chem. Soc.* **2005**, *127*, 8204–8213. [[CrossRef](#)] [[PubMed](#)]
38. Porro, C.S.; Sutcliffe, M.J.; de Visser, S.P. Quantum mechanics/molecular mechanics studies on the sulfoxidation of dimethyl sulfide by Compound I and Compound 0 of Cytochrome P450: Which is the better oxidant? *J. Phys. Chem. A* **2009**, *113*, 11635–11642. [[CrossRef](#)] [[PubMed](#)]
39. Faponle, A.S.; Quesne, M.G.; Sastri, C.V.; Banse, F.; de Visser, S.P. Differences and comparisons of the properties and reactivities of iron(III)-hydroperoxo complexes with saturated coordination sphere. *Chem. Eur. J.* **2015**, *21*, 1221–1236. [[CrossRef](#)] [[PubMed](#)]
40. Faponle, A.S.; Banse, F.; de Visser, S.P. Arene activation by a nonheme iron(III)-hydroperoxo complex: Pathways leading to phenol and ketone products. *J. Biol. Inorg. Chem.* **2016**, *21*, 453–462. [[CrossRef](#)] [[PubMed](#)]
41. Yi, X.; Conesa, A.; Punt, P.J.; Hager, L.P. Examining the role of glutamic acid 183 in chloroperoxidase catalysis. *J. Biol. Chem.* **2003**, *278*, 13855–13859. [[CrossRef](#)] [[PubMed](#)]
42. Wagenknecht, H.-A.; Woggon, W.-D. Identification of intermediates in the catalytic cycle of chloroperoxidase. *Chem. Biol.* **1997**, *4*, 367–372. [[CrossRef](#)]
43. Stone, K.L.; Behan, R.K.; Green, M.T. X-ray absorption spectroscopy of chloroperoxidase compound I: Insight into the reactive intermediate of P450 chemistry. *Proc. Natl. Acad. Sci. USA* **2005**, *102*, 16563–16565. [[CrossRef](#)] [[PubMed](#)]
44. Kim, S.H.; Perera, R.; Hager, L.P.; Dawson, J.H.; Hoffman, B.M. Rapid freeze-quench ENDOR study of chloroperoxidase Compound I: The site of the radical. *J. Am. Chem. Soc.* **2006**, *128*, 5598–5599. [[CrossRef](#)] [[PubMed](#)]
45. Green, M.T.; Dawson, J.H.; Gray, H.B. Oxoiron(IV) in chloroperoxidase compound II is basic: Implications for P450 chemistry. *Science* **2004**, *304*, 1653–1656. [[CrossRef](#)] [[PubMed](#)]
46. Ogliaro, F.; Harris, N.; Cohen, S.; Filatov, M.; de Visser, S.P.; Shaik, S. A model “rebound” mechanism of hydroxylation by cytochrome P450: Stepwise and effectively concerted pathways, and their reactivity patterns. *J. Am. Chem. Soc.* **2000**, *122*, 8977–8989. [[CrossRef](#)]
47. Ogliaro, F.; Cohen, S.; de Visser, S.P.; Shaik, S. Medium polarization and hydrogen bonding effects on Compound I of cytochrome P450: What kind of a radical is it really? *J. Am. Chem. Soc.* **2000**, *122*, 12892–12893. [[CrossRef](#)]
48. Sharma, P.K.; de Visser, S.P.; Ogliaro, F.; Shaik, S. Is the ruthenium analogue of Compound I of cytochrome P450 an efficient oxidant? A theoretical investigation of the methane hydroxylation reaction. *J. Am. Chem. Soc.* **2003**, *125*, 2291–2300. [[CrossRef](#)] [[PubMed](#)]
49. De Visser, S.P.; Tan, T.S. Is the bound substrate in nitric oxide synthase protonated or neutral and what is the active oxidant that performs substrate hydroxylation? *J. Am. Chem. Soc.* **2008**, *130*, 12961–12974. [[CrossRef](#)] [[PubMed](#)]
50. De Visser, S.P.; Porro, C.S.; Quesne, M.G.; Sainna, M.A.; Munro, A.W. Overview on recent theoretical studies discriminating the two-oxidant versus two-state-reactivity models for substrate monooxygenation by cytochrome P450 enzymes. *Curr. Top. Med. Chem.* **2013**, *13*, 2218–2232. [[CrossRef](#)] [[PubMed](#)]
51. Shaik, S.; Kumar, D.; de Visser, S.P.; Altun, A.; Thiel, W. Theoretical perspective on the structure and mechanism of cytochrome P450 enzymes. *Chem. Rev.* **2005**, *105*, 2279–2328. [[CrossRef](#)] [[PubMed](#)]

52. Cantú Reinhard, F.G.; de Visser, S.P. Biodegradation of cosmetics products: A computational study of cytochrome P450 metabolism of phthalates. *Inorganics* **2017**, *5*, 77. [[CrossRef](#)]
53. Palcic, M.M.; Rutter, R.; Araiso, T.; Hager, L.P.; Dunford, H.B. Spectrum of chloroperoxidase compound I. *Biochem. Biophys. Res. Commun.* **1980**, *94*, 1123–1127. [[CrossRef](#)]
54. Egawa, D.; Proshlyakov, T.; Miki, H.; Makino, R.; Ogura, K.; Ishimura, Y. Effects of a thiolate axial ligands on the $\pi \rightarrow \pi^*$ electronic states of oxoferryl porphyrins: A study of the optical and resonance Raman spectra of compounds I and II of chloroperoxidase. *J. Biol. Inorg. Chem.* **2001**, *6*, 46–54. [[CrossRef](#)] [[PubMed](#)]
55. Rutter, R.; Hager, L.P.; Dhonau, H.; Hendrich, M.; Valentine, J.; Debrunner, P. Chloroperoxidase compound I: Electron paramagnetic resonance and Mössbauer studies. *Biochemistry* **1984**, *23*, 6809–6816. [[CrossRef](#)] [[PubMed](#)]
56. Hoffman, B.M. Electron-nuclear double resonance spectroscopy (and electron spin-echo envelope modulation spectroscopy) in bioinorganic chemistry. *Proc. Natl. Acad. Sci. USA* **2003**, *100*, 3575–3578. [[CrossRef](#)] [[PubMed](#)]
57. Green, M.T. Evidence for sulfur-based radicals in thiolate compound I intermediates. *J. Am. Chem. Soc.* **1999**, *121*, 7939–7940. [[CrossRef](#)]
58. Anthony, J.; Grodzicki, M.; Trautwein, A.X. Local density functional study of oxoiron porphyrin complexes and their one-electron oxidised derivatives. Axial ligand effects. *J. Phys. Chem.* **1997**, *101*, 2692–2701. [[CrossRef](#)]
59. Schöneboom, J.C.; Lin, H.; Reuter, N.; Thiel, W.; Cohen, S.; Ogliaro, F.; Shaik, S. The elusive oxidant species of cytochrome P450 enzymes: Characterization by combined quantum mechanical/molecular mechanical (QM/MM) calculations. *J. Am. Chem. Soc.* **2002**, *124*, 8142–8151. [[CrossRef](#)] [[PubMed](#)]
60. Li, X.-X.; Postils, V.; Sun, W.; Faponle, A.S.; Solà, M.; Wang, Y.; Nam, W.; de Visser, S.P. Reactivity patterns of (protonated) Compound II and Compound I of Cytochrome P450: Which is the better oxidant? *Chem. Eur. J.* **2017**, *23*, 6406–6418. [[CrossRef](#)] [[PubMed](#)]
61. Vardhaman, A.K.; Sastri, C.V.; Kumar, D.; de Visser, S.P. Nonheme ferric hydroperoxo intermediates are efficient oxidants of bromide oxidation. *Chem. Commun.* **2011**, *47*, 11044–11046. [[CrossRef](#)] [[PubMed](#)]
62. Vardhaman, A.K.; Barman, P.; Kumar, S.; Sastri, C.V.; Kumar, D.; de Visser, S.P. Mechanistic insight into halide oxidation by non-heme iron complexes. Haloperoxidase versus halogenase activity. *Chem. Commun.* **2013**, *49*, 10926–10928. [[CrossRef](#)] [[PubMed](#)]
63. Van Pee, K.-H.; Dong, C.; Flecks, S.; Naismith, J.; Patallo, E.P.; Wage, T. Biological halogenation has moved far beyond haloperoxidases. *Adv. Appl. Microbiol.* **2006**, *59*, 127–157. [[CrossRef](#)] [[PubMed](#)]
64. Timmins, A.; de Visser, S.P. Enzymatic halogenases and haloperoxidases: Computational studies on mechanism and function. *Adv. Protein Chem. Struct. Biol.* **2015**, *100*, 113–151. [[CrossRef](#)] [[PubMed](#)]
65. Spreti, N.; Germani, R.; Icani, A.; Savelli, G. Stabilization of chloroperoxidase by polyethylene glycols in aqueous media: Kinetic studies and synthetic applications. *Biotechnol. Prog.* **2004**, *20*, 96–101. [[CrossRef](#)] [[PubMed](#)]
66. Quesne, M.G.; de Visser, S.P. Regioselectivity of substrate hydroxylation versus halogenation by a non-heme iron(IV)-oxo complex: Possibility of rearrangement pathways. *J. Biol. Inorg. Chem.* **2012**, *17*, 841–852. [[CrossRef](#)] [[PubMed](#)]
67. Sahu, S.; Quesne, M.G.; Davies, C.G.; Dürr, M.; Ivanović-Burmazović, I.; Siegler, M.A.; Jameson, G.N.L.; de Visser, S.P.; Goldberg, D.P. Direct observation of a non-heme iron(IV)-oxo complex that mediates aromatic C-F hydroxylation. *J. Am. Chem. Soc.* **2014**, *136*, 13542–13545. [[CrossRef](#)] [[PubMed](#)]
68. Draksharapu, A.; Angelone, D.; Quesne, M.G.; Padamati, S.K.; Gómez, L.; Hage, R.; Costas, M.; Browne, W.R.; de Visser, S.P. Identification and spectroscopic characterization of nonheme iron(III) hypochlorite intermediates. *Angew. Chem. Int. Ed.* **2015**, *54*, 4357–4361. [[CrossRef](#)] [[PubMed](#)]
69. Barman, P.; Faponle, A.S.; Vardhaman, A.K.; Angelone, D.; Löhr, A.-M.; Browne, W.R.; Comba, P.; Sastri, C.V.; de Visser, S.P. Influence of ligand architecture in tuning reaction bifurcation pathways for chlorite oxidation by nonheme iron complexes. *Inorg. Chem.* **2016**, *55*, 10170–10181. [[CrossRef](#)] [[PubMed](#)]
70. Rehder, D. The bioinorganic chemistry of vanadium. *Angew. Chem. Int. Ed. Engl.* **1991**, *30*, 148–167. [[CrossRef](#)]
71. Butler, A.; Carter, J.N.; Simpson, M.T. *Handbook of Metalloproteins*; Marcel Dekker Inc.: New York, NY, USA, 2001; pp. 153–179, ISBN 9780470869819.

72. Crans, D.C.; Smee, J.J.; Gaidamauskas, E.; Yang, L. The chemistry and biochemistry of vanadium and the biological activities exerted by vanadium compounds. *Chem. Rev.* **2004**, *104*, 849–902. [[CrossRef](#)] [[PubMed](#)]
73. Winter, J.M.; Moore, B.S. Exploring the chemistry and biology of vanadium-dependent haloperoxidases. *J. Biol. Chem.* **2009**, *284*, 18577–18581. [[CrossRef](#)] [[PubMed](#)]
74. De Boer, E.; Wever, R. The reaction mechanism of the novel vanadium-bromoperoxidase. A steady-state kinetic analysis. *J. Biol. Chem.* **1988**, *263*, 12326–12332. [[PubMed](#)]
75. Van Schijndel, J.W.P.M.; Barnett, P.; Roelse, J.; Vollenbroed, E.G.M.; Wever, R. The stability and steady state kinetics of vanadium chloroperoxidase from the fungus *Curvularia inaequalis*. *Eur. J. Biochem.* **1994**, *225*, 151–157. [[CrossRef](#)] [[PubMed](#)]
76. Messerschmidt, A.; Wever, R. X-ray structure of a vanadium-containing enzyme: Chloroperoxidase from the fungus *Curvularia inaequalis*. *Proc. Natl. Acad. Sci. USA* **1996**, *93*, 392–396. [[CrossRef](#)] [[PubMed](#)]
77. Martinez, J.S.; Carroll, G.L.; Tschirret-Guth, R.A.; Altenhoff, G.; Little, D.R.; Butler, A. On the regioselectivity of vanadium bromoperoxidase. *J. Am. Chem. Soc.* **2001**, *123*, 3289–3294. [[CrossRef](#)] [[PubMed](#)]
78. Carter-Franklin, J.N.; Butler, A. Vanadium bromoperoxidase-catalyzed biosynthesis of halogenated marine natural products. *J. Am. Chem. Soc.* **2004**, *126*, 15060–15066. [[CrossRef](#)] [[PubMed](#)]
79. Renner, M.K.; Jensen, P.R.; Fenical, W. Neomangicols: Structures and absolute stereochemistries of unprecedented halogenated sesterterpenes from a marine fungus of the genus *Fusarium*. *J. Org. Chem.* **1998**, *63*, 8346–8354. [[CrossRef](#)]
80. Borchardt, S.A.; Allain, E.J.; Michels, J.J.; Stearns, G.W.; Kelly, R.F.; McCoy, W.F. Reaction of acylated homoserine lactone bacterial signalling molecules with oxidized halogen antimicrobials. *Appl. Environ. Microbiol.* **2001**, *67*, 3174–3179. [[CrossRef](#)] [[PubMed](#)]
81. Wever, R.; Hemrika, W. *Handbook of Metalloproteins*; Messerschmidt, A., Huber, R., Wieghardt, K., Poulos, T.L., Eds.; Wiley & Sons: Chichester, UK, 2001; Volume 1, ISBN 0-471-62743-7.
82. Vilter, H. Peroxidases from *Phaeophyceae*. *Bot. Mar.* **1983**, *26*, 429–435. [[CrossRef](#)]
83. Vilter, H. Peroxidases from *Phaeophyceae*: A vanadium(V)-dependent peroxidase from *Ascophyllum nodosum*. *Phytochemistry* **1984**, *23*, 1387–1390. [[CrossRef](#)]
84. Butler, A.; Sandy, M. Mechanistic considerations of halogenating enzymes. *Nature* **2009**, *460*, 848–854. [[CrossRef](#)] [[PubMed](#)]
85. De Boer, E.; Plat, H.; Tromp, M.G.; Wever, R.; Franssen, M.C.; van der Plas, H.C.; Meijer, E.M.; Shoemaker, H.E. Vanadium containing bromoperoxidase: An example of an oxidoreductase with high operational stability in aqueous and organic media. *Biotechnol. Bioeng.* **1987**, *30*, 607–610. [[CrossRef](#)] [[PubMed](#)]
86. Coupe, E.E.; Smyth, M.G.; Fosberry, A.P.; Hall, R.M.; Littlechild, J.A. The dodecameric vanadium-dependent haloperoxidase from the marine algae *Corallina officinalis*: Cloning, expression, and refolding of the recombinant enzyme. *Protein Expr. Purif.* **2007**, *52*, 265–272. [[CrossRef](#)] [[PubMed](#)]
87. Andersson, M.; Willetts, A.; Allenmark, S. Asymmetric sulfoxidation catalyzed by a vanadium-containing bromoperoxidase. *J. Org. Chem.* **1997**, *62*, 8455–8458. [[CrossRef](#)] [[PubMed](#)]
88. Ten Brink, H.B.; Dekker, H.L.; Schoemaker, H.E.; Wever, R. Oxidation reactions catalyzed by vanadium chloroperoxidase from *Curvularia inaequalis*. *J. Inorg. Biochem.* **2000**, *80*, 91–98. [[CrossRef](#)]
89. Bernhardt, P.; Okino, T.; Winter, J.M.; Miyanaga, A.; Moore, B.S. A stereoselective vanadium-dependent chloroperoxidase in bacterial antibiotic biosynthesis. *J. Am. Chem. Soc.* **2011**, *133*, 4268–4270. [[CrossRef](#)] [[PubMed](#)]
90. Messerschmidt, A.; Prade, L.; Wever, R. Implications for the catalytic mechanism of the vanadium-containing enzyme chloroperoxidase from the fungus *Curvularia inaequalis* by X-ray structures of the native and peroxide form. *J. Biol. Chem.* **1997**, *378*, 309–315. [[CrossRef](#)]
91. Macedo-Ribeiro, S.; Hemrika, W.; Renirie, R.; Wever, R.; Messerschmidt, A. X-ray crystal structures of active site mutants of the vanadium-containing chloroperoxidase from the fungus *Curvularia inaequalis*. *J. Biol. Inorg. Chem.* **1999**, *4*, 209–219. [[CrossRef](#)] [[PubMed](#)]
92. Weyand, M.; Hecht, H.; Kiess, M.; Liaud, M.; Vitler, H.; Schomburg, D. X-ray structure determination of a vanadium-dependent haloperoxidase from *Ascophyllum nodosum* at 2.0 Å resolution. *J. Mol. Biol.* **1999**, *293*, 595–611. [[CrossRef](#)] [[PubMed](#)]
93. Isupov, M.N.; Dalby, A.R.; Brindley, A.A.; Izumi, Y.; Tanabe, T.; Murshudov, G.N.; Littlechild, J.A. Crystal structure of dodecameric vanadium-dependent bromoperoxidase from the red algae *Corallina officinalis*. *J. Mol. Biol.* **2000**, *299*, 1035–1049. [[CrossRef](#)] [[PubMed](#)]

94. Butler, A.; Carter-Franklin, J.N. The role of vanadium bromoperoxidase in the biosynthesis of halogenated marine natural products. *Nat. Prod. Rep.* **2004**, *21*, 180–188. [[CrossRef](#)] [[PubMed](#)]
95. Hemrika, W.; Renirie, R.; Macedo-Ribeiro, S.; Messerschmidt, A.; Wever, R. Heterologous Expression of the Vanadium-containing Chloroperoxidase from *Curvularia inaequalis* in *Saccharomyces cerevisiae* and Site-directed Mutagenesis of the Active Site Residues His496, Lys353, Arg360, and Arg490. *J. Biol. Chem.* **1999**, *274*, 23820–23827. [[CrossRef](#)] [[PubMed](#)]
96. Renirie, R.; Hemrika, W.; Wever, R. Peroxidase and Phosphatase Activity of Active-site Mutants of Vanadium Chloroperoxidase from the Fungus *Curvularia inaequalis*. *J. Biol. Chem.* **2000**, *275*, 11650–11657. [[CrossRef](#)] [[PubMed](#)]
97. Zampella, G.; Fantucci, P.; Pecoraro, V.L.; De Gioia, L. Reactivity of peroxo forms of the vanadium haloperoxidase cofactor. A DFT investigation. *J. Am. Chem. Soc.* **2005**, *127*, 953–960. [[CrossRef](#)] [[PubMed](#)]
98. Zampella, G.; Fantucci, P.; Pecoraro, V.L.; De Gioia, L. Insight into the catalytic mechanism of vanadium haloperoxidases. DFT investigation of vanadium cofactor reactivity. *Inorg. Chem.* **2006**, *45*, 7133–7143. [[CrossRef](#)] [[PubMed](#)]
99. Schneider, C.J.; Zampella, G.; Greco, C.; Pecoraro, V.L.; De Gioia, L. Mechanistic analysis of nucleophilic substrates oxidation by functional models of vanadium-dependent haloperoxidases: A density functional theory study. *Eur. J. Inorg. Chem.* **2007**, *2007*, 515–523. [[CrossRef](#)]
100. Waller, M.P.; Bühl, M.; Geethalakshmi, K.R.; Wang, D.; Thiel, W. 51V NMR chemical shifts calculated from QM/MM models of vanadium chloroperoxidase. *Chem. Eur. J.* **2007**, *13*, 4723–4732. [[CrossRef](#)] [[PubMed](#)]
101. Waller, M.P.; Geethalakshmi, K.R.; Bühl, M. 51V NMR chemical shifts from quantum-mechanical/molecular-mechanical models of vanadium bromoperoxidase. *J. Phys. Chem. B* **2008**, *112*, 5813–5823. [[CrossRef](#)] [[PubMed](#)]
102. Geethalakshmi, K.R.; Waller, M.P.; Thiel, W.; Bühl, M. 51V NMR chemical shifts calculated from QM/MM models of peroxo forms of vanadium haloperoxidases. *J. Phys. Chem. B* **2009**, *113*, 4456–4465. [[CrossRef](#)] [[PubMed](#)]
103. Rehder, D.; Casny, M.; Grosse, R. A vanadium-51 NMR study of the binding of vanadate and peroxovanadate to proteins. *Magn. Reson. Chem.* **2004**, *42*, 745–749. [[CrossRef](#)] [[PubMed](#)]
104. Pacios, L.F.; Gálvez, O. Active site, catalytic cycle, and iodination reactions of vanadium iodoperoxidase: A computational study. *J. Chem. Theory Comput.* **2010**, *6*, 1738–1752. [[CrossRef](#)] [[PubMed](#)]
105. Conte, V.; Coletti, A.; Floris, B.; Licini, G.; Zonta, C. Mechanistic aspects of vanadium catalysed oxidations with peroxides. *Coord. Chem. Rev.* **2011**, *255*, 2165–2177. [[CrossRef](#)]
106. Butler, A. Mechanistic considerations of the vanadium haloperoxidases. *Coord. Chem. Rev.* **1999**, *187*, 17–35. [[CrossRef](#)]
107. Van Schijndel, J.W.; Vollenbroek, E.G.; Wever, R. The chloroperoxidase from the fungus *Curvularia inaequalis*; a novel vanadium enzyme. *Biochim. Biophys. Acta* **1993**, *1161*, 249–256. [[CrossRef](#)]
108. Dairi, T.; Nakano, T.; Aisaka, K.; Katsumata, R.; Hasegawa, M. Cloning and nucleotide sequence of the gene responsible for chlorination of tetracycline. *Biosci. Biotechnol. Biochem.* **1995**, *59*, 1099–1106. [[CrossRef](#)] [[PubMed](#)]
109. Chiu, H.T.; Hubbard, B.K.; Shah, A.N.; Eide, J.; Fredenburg, R.A.; Walsh, C.T.; Khosla, C. Molecular cloning and sequence analysis of the complestatin biosynthetic gene cluster. *Proc. Natl. Acad. Sci. USA* **2001**, *98*, 8548–8553. [[CrossRef](#)] [[PubMed](#)]
110. Dong, C.; Flecks, S.; Unversucht, S.; Haupt, C.; van Pée, K.H.; Naismith, J.H. Tryptophan 7-halogenase (PrnA) structure suggests a mechanism for regioselective chlorination. *Science* **2005**, *309*, 2216–2219. [[CrossRef](#)] [[PubMed](#)]
111. Eustaquio, A.S.; Gust, B.; Luft, T.; Chater, K.F.; Heide, L. Clorobiocin biosynthesis in *Streptomyces*: Identification of the halogenase and generation of structural analogs. *Chem. Biol.* **2003**, *10*, 279–288. [[CrossRef](#)]
112. Hammer, P.E.; Hill, D.S.; Lam, S.T.; van Pee, K.H.; Ligon, J.M. Four genes from *Pseudomonas fluorescens* that encode the biosynthesis of pyrrolnitrin. *Appl. Environ. Microbiol.* **1997**, *63*, 2147–2154. [[PubMed](#)]
113. Hohaus, K.; Altmann, A.; Burd, W.; Fischer, I.; Hammer, P.E.; Hill, D.S.; Ligon, J.M.; van Pee, K.-H. NADH-dependent halogenases are more likely to be involved in halometabolite biosynthesis than haloperoxidases. *Angew. Chem. Int. Ed. Engl.* **1997**, *36*, 2012–2013. [[CrossRef](#)]

114. Keller, S.; Wage, T.; Hohaus, K.; Hölzer, M.; Eichhorn, E.; van Pée, K.H. Purification and partial characterization of tryptophan 7-halogenase(PrnA) from *Pseudomonas fluorescens*. *Angew. Chem. Int. Ed. Engl.* **2000**, *39*, 2300–2302. [[CrossRef](#)]
115. Nowak-Thompson, B.; Chaney, N.; Wing, J.S.; Gould, S.J.; Loper, J.E. Characterization of the pyoluteorin biosynthetic gene cluster of *Pseudomonas fluorescens* Pf-5. *J. Bacteriol.* **1999**, *181*, 2166–2174. [[PubMed](#)]
116. Puk, O.; Huber, P.; Bischoff, D.; Recktenwald, J.; Jung, G.; Süßmuth, R.D.; van Pee, K.-H.; Wohlleben, W.; Pelzer, S. Glycoprotein biosynthesis in *Amycolatopsis mediterranei* DSM5908: Function of a halogenase and a haloperoxidase/perhydrolase. *Chem. Biol.* **2002**, *9*, 225–235. [[CrossRef](#)]
117. Sánchez, C.; Butovich, I.A.; Brana, A.F.; Rohr, J.; Méndez, C.; Salas, J.A. The biosynthetic gene cluster for the antitumor rebeccamycin. Characterization and generation of indolocarbazole derivatives. *Chem. Biol.* **2002**, *9*, 519–531. [[CrossRef](#)]
118. Seibold, C.; Schnerr, H.; Rumpf, J.; Kunzendorf, A.; Hatscher, C.; Wage, T.; Ernyei, A.J. A flavin-dependent tryptophan 6-halogenase and its use in modification of pyrrolnitrin biosynthesis. *Biocatal. Biotransform.* **2006**, *24*, 401–408. [[CrossRef](#)]
119. Trefzer, A.; Pelzer, S.; Schimana, J.; Stockert, S.; Bihlmaier, C.; Fiedler, H.P.; Welzel, K.; Vente, A.; Bechthold, A. Biosynthetic gene cluster of simocyclinone, a natural multihybrid antibiotic. *Antimicrob. Agents Chem.* **2002**, *46*, 1174–1182. [[CrossRef](#)]
120. Weitnauer, G.; Mühlenweg, A.; Trefzer, A.; Hoffmeister, D.; Süßmuth, R.D.; Jung, G.; Welzel, K.; Vente, A.; Girreser, U.; Bechthold, A. Biosynthesis of the orthosomycin antibiotic avilamycin A: Deductions from the molecular analysis of the avi biosynthetic gene cluster of *Streptomyces viridochromogenes* Tü57 and production of new antibiotics. *Chem. Biol.* **2001**, *8*, 569–581. [[CrossRef](#)]
121. Wijnands, I.; van Pee, K.H. A novel halogenase gene from the pentachloropseudilin producer *Actinoplanes* sp. ATCC 33002 and detection of in vitro halogenase activity. *FEMS Microbiol. Lett.* **2004**, *237*, 363–367. [[CrossRef](#)]
122. Yeh, E.; Cole, L.J.; Barr, E.W.; Bollinger, J.M., Jr.; Ballou, D.P.; Walsh, C.T. Flavin redox chemistry precedes substrate chlorination during the reaction of the flavin-dependent halogenase RebH. *Biochemistry* **2006**, *45*, 7904–7912. [[CrossRef](#)] [[PubMed](#)]
123. Dong, C.; Kotzsch, A.; Dorward, M.; van Pee, K.H.; Naismith, J.H. Crystallization and X-ray diffraction of a halogenating enzyme, tryptophan 7-halogenase, from *Pseudomonas fluorescens*. *Acta Crystallogr. D* **2004**, *60*, 1438–1440. [[CrossRef](#)] [[PubMed](#)]
124. O'Hagan, D.; Schaffrath, C.; Cobb, S.L.; Hamilton, J.T.G.; Murphy, C.D. Biochemistry: Biosynthesis of an organofluorine molecule. *Nature* **2002**, *416*, 279. [[CrossRef](#)] [[PubMed](#)]
125. O'Hagan, D.; Deng, H. Enzymatic fluorination and biotechnological developments of the fluorinase. *Chem. Rev.* **2015**, *115*, 634–649. [[CrossRef](#)] [[PubMed](#)]
126. Deng, H.; Ma, L. Identification of fluorinases from *Streptomyces* sp MA37, *Nocardia brasiliensis*, and *Actinoplanes* sp N902-109 by genome mining. *Chembiochem* **2014**, *15*, 364–368. [[CrossRef](#)] [[PubMed](#)]
127. Senn, H.M. Insights into enzymatic halogenation from computational studies. *Front. Chem.* **2014**, *2*, 98. [[CrossRef](#)] [[PubMed](#)]
128. Senn, H.M.; O'Hagan, D.; Thiel, W. Insight into enzymatic C–F bond formation from QM and QM/MM calculations. *J. Am. Chem. Soc.* **2005**, *127*, 13643–13655. [[CrossRef](#)] [[PubMed](#)]
129. Aluri, S.; de Visser, S.P. The mechanism of cysteine oxygenation by cysteine dioxygenase enzymes. *J. Am. Chem. Soc.* **2007**, *129*, 14846–14847. [[CrossRef](#)] [[PubMed](#)]
130. De Visser, S.P.; Straganz, G.D. Why do cysteine dioxygenase enzymes contain a 3-His ligand motif rather than a 2His/1Asp motif like most nonheme dioxygenases? *J. Phys. Chem. A* **2009**, *113*, 1835–1846. [[CrossRef](#)] [[PubMed](#)]
131. Kumar, D.; Sastry, G.N.; Goldberg, D.P.; de Visser, S.P. Mechanism of S-oxygenation by a cysteine dioxygenase model complex. *J. Phys. Chem. A* **2012**, *116*, 582–591. [[CrossRef](#)] [[PubMed](#)]
132. Fellner, M.; Siakkou, E.; Faponle, A.S.; Tchesnokov, E.P.; de Visser, S.P.; Wilbanks, S.M.; Jameson, G.N.L. Influence of cysteine 164 on active site structure in rat cysteine dioxygenase. *J. Biol. Inorg. Chem.* **2016**, *21*, 501–510. [[CrossRef](#)] [[PubMed](#)]
133. Tchesnokov, E.P.; Faponle, A.S.; Davies, C.G.; Quesne, M.G.; Turner, R.; Fellner, M.; Souness, R.J.; Wilbanks, S.M.; de Visser, S.P.; Jameson, G.N.L. An iron-oxygen intermediate formed during the catalytic cycle of cysteine dioxygenase. *Chem. Commun.* **2016**, *52*, 8814–8817. [[CrossRef](#)] [[PubMed](#)]

134. Faponle, A.S.; Seebeck, F.P.; de Visser, S.P. Sulfoxide synthase versus cysteine dioxygenase reactivity in a nonheme iron enzyme. *J. Am. Chem. Soc.* **2017**, *139*, 9259–9270. [[CrossRef](#)] [[PubMed](#)]
135. Anderson, R.J.L.; Chapman, S.K. Molecular mechanisms of enzyme-catalysed halogenation. *Mol. BioSyst.* **2006**, *2*, 350–357. [[CrossRef](#)] [[PubMed](#)]
136. Smith, D.R.M.; Gruschow, S.; Goss, R.J.M. Scope and potential of halogenases in biosynthetic applications. *Curr. Opin. Chem. Biol.* **2013**, *17*, 276–283. [[CrossRef](#)] [[PubMed](#)]
137. Wagner, C.; Omari, M.E.; Konig, G.M. Biohalogenation: Nature's way to synthesize halogenated metabolites. *J. Nat. Prod.* **2009**, *72*, 540–553. [[CrossRef](#)] [[PubMed](#)]
138. Timmins, A.; Saint-André, M.; de Visser, S.P. Understanding how prolyl-4-hydroxylase structure steers a ferryl oxidant toward scission of a strong C-H bond. *J. Am. Chem. Soc.* **2017**, *139*, 9855–9866. [[CrossRef](#)] [[PubMed](#)]
139. Timmins, A.; de Visser, S.P. How are substrate binding and catalysis affected by mutating Glu127 and Arg161 in prolyl-4-hydroxylase? A QM/MM and MD study. *Front. Chem.* **2017**, *5*, 94. [[CrossRef](#)] [[PubMed](#)]
140. Hillwig, M.L.; Fuhrman, H.A.; Ittiarnornkul, K.; Sevco, T.J.; Kwak, D.H.; Liu, X. Identification and characterization of a welwitindolinone alkaloid biosynthetic gene cluster in the *Stigonematalean* cyanobacterium *Hapalosiphon welwitschii*. *ChemBioChem* **2014**, *15*, 665–669. [[CrossRef](#)] [[PubMed](#)]
141. Hillwig, M.L.; Liu, X. A new family of iron-dependent halogenases acts on freestanding substrates. *Nat. Chem. Biol.* **2014**, *10*, 921–923. [[CrossRef](#)] [[PubMed](#)]
142. Mitchell, A.J.; Zhu, Q.; Maggiolo, A.O.; Ananth, N.R.; Hillwig, M.L.; Liu, X.; Boal, A.K. Structural basis for halogenation by iron- and 2-oxo-glutarate-dependent enzyme WelO5. *Nat. Chem. Biol.* **2016**, *12*, 636–640. [[CrossRef](#)] [[PubMed](#)]
143. Bollinger, J.M., Jr.; Price, J.C.; Hoffart, L.M.; Barr, E.W.; Krebs, C. Mechanism of taurine: α -Ketoglutarate dioxygenase (TauD) from *Escherichia coli*. *Eur. J. Inorg. Chem.* **2005**, *2005*, 4245–4254. [[CrossRef](#)]
144. Bruijninx, P.C.A.; van Koten, G.; Klein Gebbink, R.J.M. Mononuclear non-heme iron enzymes with the 2-His-1-carboxylate facial triad: Recent developments in enzymology and modeling studies. *Chem. Soc. Rev.* **2008**, *37*, 2716–2744. [[CrossRef](#)] [[PubMed](#)]
145. De Visser, S.P. Elucidating enzyme mechanism and intrinsic chemical properties of short-lived intermediates in the catalytic cycles of cysteine dioxygenase and taurine/ α -ketoglutarate dioxygenase. *Coord. Chem. Rev.* **2009**, *253*, 754–768. [[CrossRef](#)]
146. *Iron-Containing Enzymes: Versatile Catalysts of Hydroxylation Reaction in Nature*; de Visser, S.P.; Kumar, D. (Eds.) RSC Publishing: Cambridge, UK, 2011.
147. Buongiorno, D.; Straganz, G.D. Structure and function of atypically coordinated enzymatic mononuclear non-heme-Fe(II) centers. *Coord. Chem. Rev.* **2013**, *257*, 541–563. [[CrossRef](#)] [[PubMed](#)]
148. Latifi, R.; Bagherzadeh, M.; de Visser, S.P. Origin of the correlation of the rate constant of substrate hydroxylation by nonheme iron(IV)-oxo complexes with the bond-dissociation energy of the C–H bond of the substrate. *Chem. Eur. J.* **2009**, *15*, 6651–6662. [[CrossRef](#)] [[PubMed](#)]
149. Karamzadeh, B.; Kumar, D.; Sastry, G.N.; de Visser, S.P. Steric factors override thermodynamic driving force in regioselectivity of proline hydroxylation by prolyl-4-hydroxylase enzymes. *J. Phys. Chem. A* **2010**, *114*, 13234–13243. [[CrossRef](#)] [[PubMed](#)]
150. de Visser, S.P.; Latifi, R.; Tahsini, L.; Nam, W. The axial ligand effect on aliphatic and aromatic hydroxylation by nonheme iron(IV)-oxo biomimetic complexes. *Chem. Asian J.* **2011**, *6*, 493–504. [[CrossRef](#)] [[PubMed](#)]
151. Pratter, S.M.; Konstantinovic, C.; DiGiuro, C.L.M.; Leitner, E.; Kumar, D.; de Visser, S.P.; Grogan, G.; Straganz, G.D. Inversion of enantio-selectivity of a mononuclear non-heme iron(II)-dependent hydroxylase by tuning the interplay of metal-center geometry and protein structure. *Angew. Chem. Int. Ed.* **2013**, *52*, 9677–9681. [[CrossRef](#)] [[PubMed](#)]
152. Jastrzebski, R.; Quesne, M.G.; Weckhuysen, B.M.; de Visser, S.P.; Bruijninx, P.C.A. Experimental and computational evidence for the mechanism of intradiol catechol dioxygenation by non-heme iron(III) complexes. *Chem. Eur. J.* **2014**, *20*, 15686–15691. [[CrossRef](#)] [[PubMed](#)]
153. Sallmann, M.; Kumar, S.; Chernev, P.; Nehrkorn, J.; Schnegg, A.; Kumar, D.; Dau, H.; Limberg, C.; de Visser, S.P. Structure and mechanism leading to formation of the cysteine sulfinic acid product complex of a biomimetic cysteine dioxygenase model. *Chem. Eur. J.* **2015**, *21*, 7470–7479. [[CrossRef](#)] [[PubMed](#)]

154. Kaczmarek, M.A.; Malhotra, A.; Balan, G.A.; Timmins, A.; de Visser, S.P. Nitrogen reduction to ammonia on a biomimetic mononuclear iron center: Insights into the nitrogenase enzyme. *Chem. Eur. J.* **2018**, *24*, 5293–5302. [[CrossRef](#)] [[PubMed](#)]
155. Price, J.C.; Barr, E.W.; Glass, T.E.; Krebs, C.; Bollinger, J.M., Jr. The first direct characterization of a high-valent iron intermediate in the reaction of an α -ketoglutarate-dependent dioxygenase: A high-spin Fe(IV) complex in taurine/ α -ketoglutarate dioxygenase (TauD) from *Escherichia coli*. *J. Am. Chem. Soc.* **2003**, *125*, 13008–13009. [[CrossRef](#)] [[PubMed](#)]
156. Grzyska, P.K.; Ryle, M.J.; Monterosso, G.R.; Liu, J.; Ballou, D.P.; Hausinger, R.P. Steady-state and transient kinetic analysis of taurine/ α -ketoglutarate dioxygenase: Effects of oxygen concentration, alternative sulfonates, and active-site variants on the Fe^{IV}-oxo intermediate. *Biochemistry* **2005**, *44*, 3845–3855. [[CrossRef](#)] [[PubMed](#)]
157. Abu-Omar, M.M.; Loaiza, A.; Hontzas, N. Reaction mechanisms of mononuclear non-heme iron oxygenases. *Chem. Rev.* **2005**, *105*, 2227–2252. [[CrossRef](#)] [[PubMed](#)]
158. De Visser, S.P. Propene activation by the oxo-iron active species of taurine/ α -ketoglutarate dioxygenase (TauD) enzyme. How does the catalysis compare to heme-enzymes? *J. Am. Chem. Soc.* **2006**, *128*, 9813–9824. [[CrossRef](#)] [[PubMed](#)]
159. De Visser, S.P. Trends in substrate hydroxylation reactions by heme and nonheme iron(IV)-oxo oxidants give correlations between intrinsic properties of the oxidant with barrier height. *J. Am. Chem. Soc.* **2010**, *132*, 1087–1097. [[CrossRef](#)] [[PubMed](#)]
160. Borowski, T.; Bassan, A.; Siegbahn, P.E.M. 4-Hydroxyphenylpyruvate dioxygenase: A hybrid density functional study of the catalytic reaction mechanism. *Biochemistry* **2004**, *43*, 12331–12342. [[CrossRef](#)] [[PubMed](#)]
161. De Visser, S.P. Can the peroxosuccinate complex in the catalytic cycle of taurine/ α -ketoglutarate dioxygenase (TauD) act as an alternative oxidant? *Chem. Commun.* **2007**, 171–173. [[CrossRef](#)] [[PubMed](#)]
162. Godfrey, E.; Porro, C.S.; de Visser, S.P. Comparative quantum mechanics/molecular mechanics (QM/MM) and density functional theory calculations on the oxo-iron species of taurine/ α -ketoglutarate dioxygenase. *J. Phys. Chem. A* **2008**, *112*, 2464–2468. [[CrossRef](#)] [[PubMed](#)]
163. Quesne, M.G.; Latifi, R.; Gonzalez-Ovalle, L.E.; Kumar, D.; de Visser, S.P. Quantum mechanics/molecular mechanics study on the oxygen binding and substrate hydroxylation step in AlkB repair enzymes. *Chem. Eur. J.* **2014**, *20*, 435–446. [[CrossRef](#)] [[PubMed](#)]
164. Diebold, A.R.; Brown-Marshall, C.D.; Neidig, M.L.; Brownlee, J.M.; Moran, G.R.; Solomon, E.I. Activation of α -keto acid-dependent dioxygenases: Application of an $\{FeNO\}^7/\{FeO_2\}^8$ methodology for characterizing the initial steps of O₂ activation. *J. Am. Chem. Soc.* **2011**, *133*, 18148–18160. [[CrossRef](#)] [[PubMed](#)]
165. Borowski, T.; Bassan, A.; Siegbahn, P.E.M. Mechanism of dioxygen activation in 2-oxoglutarate-dependent enzymes. A hybrid DFT study. *Chem. Eur. J.* **2004**, *10*, 1031–1041. [[CrossRef](#)] [[PubMed](#)]
166. Topol, I.A.; Nemukhin, A.V.; Salnikow, K.; Cachau, R.E.; Abashkin, Y.G.; Kasprzak, K.S.; Burt, S.K. Quantum chemical modeling of reaction mechanism for 2-glutarate dependent enzymes: Effect of substitution of iron by nickel and cobalt. *J. Phys. Chem. A* **2006**, *110*, 4223–4228. [[CrossRef](#)] [[PubMed](#)]
167. Ye, S.; Riplinger, C.; Hansen, A.; Krebs, C.; Bollinger, J.M., Jr.; Neese, F. Electronic structure analysis of the oxygen-activation mechanism by Fe^{II}- and α -ketoglutarate (α KG)-dependent dioxygenases. *Chem. Eur. J.* **2012**, *18*, 6555–6567. [[CrossRef](#)] [[PubMed](#)]
168. Matthews, M.L.; Krest, C.M.; Barr, E.W.; Vaillancourt, F.H.; Walsh, C.T.; Green, M.T.; Krebs, C.; Bollinger, J.M., Jr. Substrate-triggered formation and remarkable stability of the C-H bond-cleaving chloroferryl intermediate in the aliphatic halogenase, SyrB2. *Biochemistry* **2009**, *48*, 4331–4343. [[CrossRef](#)] [[PubMed](#)]
169. Matthews, M.L.; Neumann, C.S.; Miles, L.A.; Grove, T.L.; Booker, S.J.; Krebs, C.; Walsh, C.T.; Bollinger, J.M., Jr. Substrate positioning controls the partition between halogenation and hydroxylation in the aliphatic halogenase, SyrB2. *Proc. Natl. Acad. Sci. USA* **2009**, *106*, 17723–17728. [[CrossRef](#)] [[PubMed](#)]
170. Kulik, H.J.; Drennan, C.L. Substrate placement influences reactivity in non-heme Fe(II) halogenases and hydroxylases. *J. Biol. Chem.* **2013**, *288*, 11233–11241. [[CrossRef](#)] [[PubMed](#)]
171. Wong, S.D.; Srncic, M.; Matthews, M.L.; Liu, L.V.; Kwak, Y.; Park, K.; Bell, C.B.; Alp, E.; Zhao, J.; Yoda, Y.; et al. Elucidation of the Fe(IV)=O intermediate in the catalytic cycle of the halogenase SyrB2. *Nature* **2013**, *499*, 320–323. [[CrossRef](#)] [[PubMed](#)]

172. Pandian, S.; Vincent, M.A.; Hillier, I.H.; Burton, N.A. Why does the enzyme SyrB2 chlorinate, but does not hydroxylate, saturated hydrocarbons? A density functional theory (DFT) study. *Dalton Trans.* **2009**, *31*, 6201–6207. [[CrossRef](#)] [[PubMed](#)]
173. Kulik, H.J.; Blasiak, L.C.; Marzari, N.; Drennan, C.L. First-principles study of non-heme Fe(II) halogenase SyrB2 reactivity. *J. Am. Chem. Soc.* **2009**, *131*, 14426–14433. [[CrossRef](#)] [[PubMed](#)]
174. De Visser, S.P.; Latifi, R. Carbon dioxide: A waste product in the catalytic cycle of alpha-ketoglutarate dependent halogenases prevents the formation of hydroxylated by-products. *J. Phys. Chem. B* **2009**, *113*, 12–14. [[CrossRef](#)] [[PubMed](#)]
175. Kojima, T.; Leising, R.A.; Yan, S.; Que, L., Jr. Alkane functionalization at nonheme iron centers. Stoichiometric transfer of metal-bound ligands to alkane. *J. Am. Chem. Soc.* **1993**, *115*, 11328–11335. [[CrossRef](#)]
176. Borowski, T.; Noack, H.; Radon, M.; Zych, K.; Siegbahn, P.E.M. Mechanism of selective halogenation by SyrB2: A computational study. *J. Am. Chem. Soc.* **2010**, *132*, 12887–12898. [[CrossRef](#)] [[PubMed](#)]
177. Huang, J.; Li, C.; Wang, B.; Sharon, D.A.; Wu, W.; Shaik, S. Selective chlorination of substrates by the halogenase SyrB2 is controlled by the protein according to a combined quantum mechanics/molecular mechanics and molecular dynamics study. *ACS Catal.* **2016**, *6*, 2694–2704. [[CrossRef](#)]
178. Timmins, A.; Fowler, N.J.; Warwicker, J.; Straganz, G.D.; de Visser, S.P. Does substrate positioning affect the selectivity and reactivity in the hectochlorin biosynthesis halogenase? 2018; Submitted for publication.
179. Srncic, M.; Solomon, E.I. Frontier molecular orbital contributions to chlorination versus hydroxylation selectivity in the non-heme iron halogenase SyrB2. *J. Am. Chem. Soc.* **2017**, *139*, 2396–2407. [[CrossRef](#)] [[PubMed](#)]
180. Pratter, S.M.; Light, K.M.; Solomon, E.I.; Straganz, G.D. The role of chloride in the mechanism of O₂ activation at the mononuclear nonheme Fe(II) center of the halogenase HctB. *J. Am. Chem. Soc.* **2014**, *136*, 9385–9395. [[CrossRef](#)] [[PubMed](#)]
181. Pratter, S.M.; Ivkovic, J.; Birner-Gruenberger, R.; Breinbauer, R.; Zangger, K.; Straganz, G.D. More than just a halogenase: Modification of fatty acyl moieties by a trifunctional metal enzyme. *ChemBioChem* **2014**, *15*, 567–574. [[CrossRef](#)] [[PubMed](#)]
182. Quesne, M.G.; Borowski, T.; de Visser, S.P. Quantum mechanics/molecular mechanics modelling of enzymatic processes: Caveats and breakthroughs. *Chem. Eur. J.* **2016**, *22*, 2562–2581. [[CrossRef](#)] [[PubMed](#)]
183. Kumar, D.; Thiel, W.; de Visser, S.P. Theoretical study on the mechanism of the oxygen activation process in cysteine dioxygenase enzymes. *J. Am. Chem. Soc.* **2011**, *133*, 3869–3882. [[CrossRef](#)] [[PubMed](#)]
184. Hernández-Ortega, A.; Quesne, M.G.; Bui, S.; Heuts, D.P.H.M.; Steiner, R.A.; Heyes, D.J.; de Visser, S.P.; Scrutton, N.S. Origin of the proton-transfer step in the cofactor-free 1-H-3-hydroxy-4-oxoquinaldine 2,4-dioxygenase: Effect of the basicity of an active site His residue. *J. Biol. Chem.* **2014**, *289*, 8620–8632. [[CrossRef](#)] [[PubMed](#)]
185. Hernández-Ortega, A.; Quesne, M.G.; Bui, S.; Heyes, D.J.; Steiner, R.A.; Scrutton, N.S.; de Visser, S.P. Catalytic mechanism of cofactor-free dioxygenases and how they circumvent spin-forbidden oxygenation of their substrates. *J. Am. Chem. Soc.* **2015**, *137*, 7474–7487. [[CrossRef](#)] [[PubMed](#)]
186. Faponle, A.S.; Quesne, M.G.; de Visser, S.P. Origin of the regioselective fatty acid hydroxylation versus decarboxylation by a cytochrome P450 peroxygenase: What drives the reaction to biofuel production: What Drives the Reaction to Biofuel Production? *Chem. Eur. J.* **2016**, *22*, 5478–5483. [[CrossRef](#)] [[PubMed](#)]
187. Sainna, M.A.; Kumar, S.; Kumar, D.; Fornarini, S.; Crestoni, M.E.; de Visser, S.P. A comprehensive test set of epoxidation rate constants by iron(IV)-oxo porphyrin complexes. *Chem. Sci.* **2015**, *6*, 1516–1529. [[CrossRef](#)] [[PubMed](#)]
188. Sainna, M.A.; Sil, D.; Sahoo, D.; Martin, B.; Rath, S.P.; Comba, P.; de Visser, S.P. Spin state ordering in hydroxo-bridged diiron(III)bisporphyrin complexes. *Inorg. Chem.* **2015**, *54*, 1919–1930. [[CrossRef](#)] [[PubMed](#)]
189. Yang, T.; Quesne, M.G.; Neu, H.M.; Cantú Reinhard, F.G.; Goldberg, D.P.; de Visser, S.P. Singlet versus triplet reactivity in an Mn(V)-Oxo species: Testing theoretical predictions against experimental evidence. *J. Am. Chem. Soc.* **2016**, *138*, 12375–12386. [[CrossRef](#)] [[PubMed](#)]
190. Cantú Reinhard, F.G.; Sainna, M.A.; Upadhyay, P.; Balan, G.A.; Kumar, D.; Fornarini, S.; Crestoni, M.E.; de Visser, S.P. A systematic account on aromatic hydroxylation by a cytochrome P450 model Compound I: A low-pressure mass spectrometry and computational study. *Chem. Eur. J.* **2016**, *22*, 18608–18619. [[CrossRef](#)] [[PubMed](#)]

191. Cantú Reinhard, F.G.; Faponle, A.S.; de Visser, S.P. Substrate sulfoxidation by an iron(IV)-oxo complex: Benchmarking computationally calculated barrier heights to experiment. *J. Phys. Chem. A* **2016**, *120*, 9805–9814. [[CrossRef](#)] [[PubMed](#)]
192. Fowler, N.J.; Blanford, C.F.; Warwicker, J.; de Visser, S.P. Prediction of reduction potentials of copper proteins with continuum electrostatics and density functional theory. *Chem. Eur. J.* **2017**, *23*, 15436–15445. [[CrossRef](#)] [[PubMed](#)]
193. Cantú Reinhard, F.G.; Fornarini, S.; Crestoni, M.E.; de Visser, S.P. Hydrogen atom versus hydride transfer in cytochrome P450 oxidations: A combined mass spectrometry and computational study. *Eur. J. Inorg. Chem.* **2018**, *2018*, 1854–1865. [[CrossRef](#)]
194. Swart, M. Accurate spin-state energies for iron complexes. *J. Chem. Theory Comput.* **2008**, *4*, 2057–2066. [[CrossRef](#)] [[PubMed](#)]
195. De Visser, S.P.; Kumar, D.; Cohen, S.; Shacham, R.; Shaik, S. A predictive pattern of computed barriers for C–H hydroxylation by Compound I of cytochrome P450. *J. Am. Chem. Soc.* **2004**, *126*, 8362–8363. [[CrossRef](#)] [[PubMed](#)]
196. De Visser, S.P.; Kumar, D.; Neumann, R.; Shaik, S. Computer-generated high-valent iron-oxo and manganese-oxo species with polyoxometalate ligands: How do they compare with the iron-oxo active species of heme enzymes? *Angew. Chem. Int. Ed.* **2004**, *43*, 5661–5665. [[CrossRef](#)] [[PubMed](#)]
197. De Visser, S.P. Differences in and comparison of the catalytic properties of heme and non-heme enzymes with a central oxo-iron group. *Angew. Chem. Int. Ed.* **2006**, *45*, 1790–1793. [[CrossRef](#)] [[PubMed](#)]
198. De Visser, S.P. Substitution of hydrogen by deuterium changes the regioselectivity of ethylbenzene hydroxylation by an oxo-iron-porphyrin catalyst. *Chem. Eur. J.* **2006**, *12*, 8168–8177. [[CrossRef](#)] [[PubMed](#)]
199. De Visser, S.P. What factors influence the ratio of C–H hydroxylation versus C=C epoxidation by a nonheme cytochrome P450 biomimetic? *J. Am. Chem. Soc.* **2006**, *128*, 15809–15818. [[CrossRef](#)] [[PubMed](#)]
200. Kumar, S.; Faponle, A.S.; Barman, P.; Vardhaman, A.K.; Sastri, C.V.; Kumar, D.; de Visser, S.P. Long-range electron transfer triggers mechanistic differences between iron(IV)-oxo and iron(IV)-imido oxidants. *J. Am. Chem. Soc.* **2014**, *136*, 17102–17115. [[CrossRef](#)] [[PubMed](#)]
201. Ji, L.; Faponle, A.S.; Quesne, M.G.; Sainna, M.A.; Zhang, J.; Franke, A.; Kumar, D.; van Eldik, R.; Liu, W.; de Visser, S.P. Drug metabolism by cytochrome P450 enzymes: What distinguishes the pathways leading to substrate hydroxylation over desaturation? *Chem. Eur. J.* **2015**, *21*, 9083–9092. [[CrossRef](#)] [[PubMed](#)]
202. Barman, P.; Upadhyay, P.; Faponle, A.S.; Kumar, J.; Nag, S.S.; Kumar, D.; Sastri, C.V.; de Visser, S.P. Deformylation reaction by a nonheme manganese(III)-peroxo complex via initial hydrogen atom abstraction. *Angew. Chem. Int. Ed.* **2016**, *55*, 11091–11095. [[CrossRef](#)] [[PubMed](#)]
203. Cantú Reinhard, F.G.; de Visser, S.P. Oxygen atom transfer using an iron(IV)-oxo embedded in a tetracyclic N-heterocyclic carbene system: How does the reactivity compare to Cytochrome P450 Compound I? *Chem. Eur. J.* **2017**, *23*, 2935–2944. [[CrossRef](#)] [[PubMed](#)]
204. Cantú Reinhard, F.G.; Barman, P.; Mukherjee, G.; Kumar, J.; Kumar, D.; Kumar, D.; Sastri, C.V.; de Visser, S.P. Keto-enol tautomerization triggers an electrophilic aldehyde deformylation reaction by a nonheme manganese(III)-peroxo complex. *J. Am. Chem. Soc.* **2017**, *139*, 18328–18338. [[CrossRef](#)] [[PubMed](#)]
205. Shaik, S.; Kumar, D.; de Visser, S.P. A valence bond modeling of trends in hydrogen abstraction barriers and transition states of hydroxylation reactions catalyzed by cytochrome P450 enzymes. *J. Am. Chem. Soc.* **2008**, *130*, 10128–10140. [[CrossRef](#)] [[PubMed](#)]
206. Heyes, D.J.; Sakuma, M.; de Visser, S.P.; Scrutton, N.S. Nuclear quantum tunneling in the light-activated enzyme protochlorophyllide oxidoreductase. *J. Biol. Chem.* **2009**, *284*, 3762–3767. [[CrossRef](#)] [[PubMed](#)]
207. Vardhaman, A.K.; Barman, P.; Kumar, S.; Sastri, C.V.; Kumar, D.; de Visser, S.P. Comparison of the reactivity of nonheme iron(IV)-oxo versus iron(IV)-imido complexes: Which is the better oxidant? *Angew. Chem. Int. Ed.* **2013**, *52*, 12288–12292. [[CrossRef](#)] [[PubMed](#)]
208. Quesne, M.G.; Senthilnathan, D.; Singh, D.; Kumar, D.; Maldivi, P.; Sorokin, A.B.; de Visser, S.P. Origin of the enhanced reactivity of μ -nitrido-bridged diiron(IV)-oxo porphyrinoid complexes over cytochrome P450 Compound I. *ACS Catal.* **2016**, *6*, 2230–2243. [[CrossRef](#)]

